9

NASICON: Synthesis, Structure and Electrical Characterization

Umaru Ahmadu

Department of Physics, Federal University of Technology, Minna, Nigeria

Abstract

NASICON (Na-Super-Ioni-CONductor) has the general formula $Na_{1-x}Zr_2P_{3-x}Si_xO_{12}$ ($0 \leq x \leq 3$) and is derived from the parent compound sodium zirconium phosphate, $NaZr_2(PO_4)_3$, i.e., NZP. It belongs to the class of superionic conductors, materials that have high ionic conductivity at elevated or room temperatures, similar to those of liquid electrolytes at room temperatures. NASICON is special due to its unique structural features (three-dimensional), which confer on it high conductivity and diverse physical and chemical characteristics suitable for various applications in many fields. The Na, Zr and P can be substitutted by atoms of differing sizes and oxidation states, up to about forty or more of such atoms, leading to its tailorability for targetted applications in recahargeable lithium ion batteries, gas sensors, low-zero-and even negative thermal expansion materials, nuclear waste immobilization, among others. In the present work we survey some classes of ionic conductors and the theoretical models of their conduction. A review of the electrical conductivity, dielectric relaxation, methods of synthesis, together with characterization techniques of NASICON, DTA/TGA, Impedance spectroscopy, NMR, FT-IR, among others, are highlighted. Case studies of some experimental results have been presented.

Keywords: NASICON, superionic conductors, theoretical models, synthesis, structure and electrical properties

9.1 Introduction

Ionic materials are in recent times at the forefront of materials research. They are part and parcel of our electronic industry in that they complement

**Corresponding author*: u.ahmadu@yahoo.com

Ashutosh Tiwari and Mustafa M. Demir (eds.) Advanced Sensor and Detection Materials, (265–308)

the all-ubiquitous electronically-based semiconductor devices as a result of the alternative they offer as renewable energy sources, low cost, environmental friendliness, flexibility, and potential applications. They are used in various applications such as rechargeable lithium ion batteries for laptop computers, mobile phones, and as electrodes and electrolyte materials. As electrolytes, the materials should have high room temperature ionic conductivity, transference number close to 1 and temperature stability, among others [1–3]. Whearas as electrodes they should have mixed conduction properties, i.e., electronic and ionic. Superionic conductors are materials whose electrical conductivity approaches that of liquid electrolytes at high and room temperatures, with their conductivity approaching that of the molten state or acqueous solution at room temperature, of the order of 10^{-1} to 10^{-3} S/m [4]. The conductivity is due to delocalization of one or more of the ionic species in the sublattice of the framework structure of the materials, which move them under an applied electric field. The mobile ions are usually Li^+ or Na^+ and are generally monovalent and cationic. However, recently [5] high Hf^{4+} ion conductivity in $HfNbP_{3-x}V_xO_{12}$ and $Hf_{1-y/4}NbP_{3-y}W_yO_{12}$, by partially replacing the P^{5+} site in a $HfNb(PO_4)_3$ solid with larger V^{5+} or W^{6+} ions through lattice volume expansion, has been demonstrated. The highest conductivity of 2.8×10^{-2} S m^{-1} at 873 K was recorded in the systems. Anionic mobile ions can also conduct electricity in compounds like ZrO_2, Ce_2O_3, AgF, among others, where O^{2-} and F^- are the principal mobile species. Such is the case in Solid Oxide Fuel cells (SOFCs), which normally operate at high temperatures, ~873 K, so-called intermediate temperature [6], e.g., yitrium stabilized zirconia.

Ionic conductors may be solid, glassy, or polymer in nature, property that gives them a good advantage over the liquid electrolytes. Glassy ionics are very important due to their high conductivity and have been widely studied as a result of their potential applications [1, 7]. The conductivity in these compounds is enhanced on introduction of a crystalline phase into the superionic glass matrix [8]. Work has also been reported on polymer electrolytes and biopolymers, with the latter reported to show evidence of superionic properties in gum Arabica [9]. Side-by-side with these developments is the trend in miniaturization of these materials, which has resulted in the new field of nanoionics [10] and their subsequent fabrication into thin films [11] due to their enormous advantages. The production of thin films of NASICON at relatively low temperatures with good physical properties has recently been reported, together with other alternative methods of production of the thin films of NASICON [12].The high conductivity in superionic conductors is due to thermal activation often associated

with phase transitions to a structural state that enhances conductivity by several orders of magnitude. Structural phase change may be related to particle size [7] and pressure, density, and microstructure affect the electrical performance of these materials. A principal challenge in this area is their electrical characterization, i.e, how to reduce the conducting temperature to ambient conditions so that they can be favorable for applications, together with an understanding and development of the appropriate theoretical models that would explain their superionic character from the microscopic point of view. Further, the appropriate synthesis of these materials is also very important in order to obtain materials with the desired physical and chemical characteristics. We focus our discussions on the physical properties of the family of ionic conductors called NASICON (Na-Super-Ioni-CON-ductor), which have been synthesized by various methods in order to optimize their electrical and microstructural properties [13–15].

Zirconium phosphate, $NaZr_2(PO_4)_3$, so–called NZP, is a member of a broad family of compounds known as NASICON ($Na_{1+x}Zr_2P_{3-x}Si_xO_{12}$) ($0 \leq x \leq 3$), where the P has been partially replaced by Si and a further addition has been made to the Na to balance the overall charge of the system (P^{5+}, Si^{4+}). Henceforth, NZP shall refer to the former chemical formula while NASICON shall refer to the latter, unless otherwise stated. NZP structure [16] was first determined by Hangman and Kierkegaad in 1967 and belongs to the rhombohedral crystal system with several interesting features and potential applications, some of which include high ionic conductivity [3], low thermal expansion coefficient [16–18], thermodynamic stability [19], nuclear waste immobilization potentials [15, 20] and use in environmental gas sensors for detection of pollutant gases [21, 22]. NZP has other potential applications in the automobile industries, e.g., for block engines and exhaust pipes of cars, space telescope technology, catalysts and catalytic supports [19], among others. It also has a unique property of enormously varied ionic substitution in its structure, accomodating forty to forty-five elements in the periodic table in its lattice without altering the basic structure [15]. Some of the elements that can be substituted in the NZP include: Li, Cs, Ca, Ba, and others for Na; Ti, Ge, Hf for Zr and Si for P. The stability of the structure for a wide range of chemical elements makes it a universal sponge for nuclear waste host material [15, 20]. The electrical properties of these materials are of considerable interest in that by replacing P with Si in NASICON, a material is produced that rivals β - alumina, one of the best Na ion conductors, for industrial solid state electrolyte applications in high temperature batteries.

9.2 Theretical Survey of Superionic Conduction

Many theoretical approaches have evolved over the years which have been successfully applied to some of these materials and have reproduced the experimental details, particularly for one-dimensional systems. Challenges, however, remain in the understanding of the origin of this behavior and in particular in the case of three-dimensional NASICON materials, thus spurring a lot of theoretical postulations to explain the conductivity mechanisms and other properties. Propositions have been put forward to study and explain the superionic phenomena in simple binary ionic systems and complex ones. We shall review some of the highpoints, including modeling and simulation techniques as general background to understanding NASICON.

An indepth review of various classes of superionic conductors, their properties and theoretical models, particularly the AgX (X = Cl, Br, I) family, have been reported [23]. Most of the models demonstrate a good correlation with experimental data, though in certain superionics such as glasses, non-Arrhenius behavior in their d.c. conductivities have been observed and appropriate theoretical models have been proposed which explained most of them [24]. Ionic materials have also been categorized into classes by conduction mechanisms and characterization techniques [25] for ease of analysis, with the authors emphasizing the increasing power and use of simulation [26, 27] techniques, such as Monte Carlo (MC) and Molecular Dynamics (MD), among others, for studying the properties of NASICON and related ionic materials. The application of these techniques in the determination of the electrical conductivity and phase transition temperature of $LiZr_2(PO_4)_3$, among others, were extensively reviewed and accurate results were obtained, which compare favorably with experimental values, such as the case of CaF_2 [28].

One of the most widely studied ionic materials is zirconia, stabilized in its high-temperature cubic form. Molecular dynamics simulation and static dynamics have been applied to study the grain boundary conductivity, producing very good results, which correlates with experimental values [29]. Other simulation techniques have been discussed [30] and the mode of implimentation and conditions of use explained, together with their applications in highly disordered systems such as CaF_2, AgI, CeO_2, and ZrO_2. These provided very valuable data on the phase transition temperatures and conductivity. The application of quantum mechanical density functional theory (DFT) [25, 30–32] in the MD simulations of these materials and similar ones have also been carried out. Atomic dynamics have been studied in superionic conductors by *ab initio* MD technique on

CuI, Ag_2Se, and the ionic conductivity was successfully reproduced [33], including the temperature dependence of the diffusion coefficient of the mobile ions, in good agreement with experimental data.

The determination of phase transition temperatures in superionic conductors is important as it is associated with a large increase in conductivity due to changes in activation energy, specific heat, among other parameters. However, some reports indicate such a transition could take place without any changes in activation energy, contrary to the expected results [34]. Many physical properties of materials change with structural transformations; however, in superionic conductors, a high conductivity is associated with this state and the increase in conductivity is abrupt and first order. NZP is not associated with structural phase transformation at the high conducting state or specific heat changes [19] in the temperature range 298 to 1123 K. These transitions could be detected accurately using photoacoustic technique [35] as it has been applied successfully to many superionic materials of the AgX family and the results agreed well with literature data on superionic transition temperatures. Work has also been carried out on how to increase the room temperature conductivity to between 10 to 10^{-1} S/m [4] or 10 to 10^{-3} S/m [36], the range that will make it suitable for applications in devices such as lithium ion batteries, with the suggestion that the non-Arrhenius behavior observed in glassy ionic conductors, which limits their conductivity, could be improved by annealing and densification of the electrolytes, since it reduces the saturation that may be responsible for the loss of Arrhenius behavior [37].

Study of the ionic conductivity of $(1\text{-}x)Li_2SO_4{:}(x)Me_2SO_4$ (where Me = Na, K, Rb, and Ag; x= 0.025 to 0.09) investigated by impedance spectroscopy [38] found that partial replacement of Li^+ with Me^+ of bigger ionic size increases the conductivity due to lattice loosening, and maximum conductivity enhancement was achieved by Ag^+ substitution. Application of a simple model based on change in entropy and Coulomb interaction found that in addition to valence, the ionic size and electronic structure of doped cations play an important role in ion transport through solid and that the mismatch in the ionic radii of host and guest cations altered inter-ionic distance and so influenced Coulomb interactions and internal energy associated with lattice vibration. A Space Charge Potential model used in the study of $BaCe_{0.8}Y_{0.2}O_{2.9-\delta}$ and cerium oxide [39, 40], respectively, showed that in ionic compounds the composition at the surface or interface may differ from that in the bulk, resulting in a difference in electric potential between the grain boundary and the bulk due to the presence of excess ions at the grain boundary under equilibrium. This is due to space charge potential developed to compensate for the excess charges. Other studies

highlighted the role played by carrier concentration, mobility, temperature, dynamics, and compositions in order to understand their high values of ionic conductivity [37].

Using a Chemical Bond approach [41], three conditions have been enumerated for a material to exhibit the superionic character: 1) it must have an open structure within which the mobile ion should have low coordination number; 2) the superionic conducting material must show a structural phase transition at relatively low pressures and 3) for a material composed of atoms A and B, a parameter defined as $z^* = \sqrt{Z_A \frac{Z_B}{\varepsilon_0}}$ exhibits a small value, where Z_A, Z_B are the valencies and ε_0 is the static dielectric constant. These criteria have been fulfilled by many superionic materials from experimental data. Other conditions include that the empty and occupied sites should have similar energies with a low activation energy for jumping between neighboring sites; that the structure should have a framework, preferably 3D, which is fulfilled by NASICON, with open channels through which ions could migrate; and that the anion framework should be highly polarizable [42], among others.

Another model is that of "coupling and decoupling" by Angel [4], which is a guideline for searching for high ionic conductivity in complex materials. The model assumes the mobile ion should be decoupled from the surrounding other ions and molecules by optimizing the chemical bond strength and coordination number. A good example is found in the so-called "mixed ion effect," where ionic conductivity shows drastic decrease when two mobile ions are mixed or present in the same substance, e.g., Na and Li in B_2O_3 glasses. The mobile ion is found to be decoupled from the surrounding counter anions to allow the ion to move fast. However, the observed conductivity shows very low values, almost insulating in some compositions. This anomalous behavior of conductivity is believed to be related to a "percolation transition," which is a special feature of complex materials not observed in simple liquids or single crystals of homogenous structure.

Real Space Pseudo Potential [41] method has been applied to study Cu and Ag Halides with the zinc-blende structure, using the Bond Model from the electronic theory of superionic conductors, which provided further insight into the concept of a "mobile ion in a cage formed by the immobile ion." In a related study [43] using the the Pseudo Potential method, AgI, a well-known superionic conductor and GaAs, a well-known semiconductor, results show that the bonding in AgI is mainly determined by the iodine and suggests that the local electronic excitations from the bonding to the

antibonding orbitals can trigger the migration of the mobile ion species and thus initiate the superionic transport. Recent interest in the electron substructure [44, 45] to explain the behavior of superionic materials led to a suggestion that the change of bonding that occurs locally and fluctuates in time plays an important role in the understanding of the phenomenon of superionic conduction. This is because the fluctuation of the bond creates fields of forces which move the ions and which in turn trigger new bond fluctuations. The model has been used successfully and applied in the interpretation of many experimental observations. Another major area of ionic conductors currently receiving attention is composites. Composite materials are heteregenous mixtures of various phases. Work on the review [46] of the theoretical framework of the ionic conduction in various classes of these materials at the interface, ion trapping, depletion levels and their relationship to conductivity changes has also been reported.

There is the screening concept and strain [47] in ionic conductors, which are relevant for the understanding of the defect and thermal properties of these compounds due to their relationship to conductivity, amongst many other contending theories of ionic conduction. In summary, the theoretical implications show that many factors affect ion motion: concentration of charge carriers, defects or mobile ions, the distance between available positions, temperature, the correlation between charge carriers, the change of the thermodynamic potential of the motion of ions, and the change of thermodynamic potential of origin of defects [48].

9.3 NASICON Synthesis

NASICON has been synthesized by many routes depending on the application in view, stability, and parameters reguired. Nanocrystalline and thin films [49–51] have been prepared but most have been prepared in polycrystalline (microcrystalline) forms due to various advantages. Some of the methods of preparation are solid state reaction [52, 69], solution–gel [53–55], hydrothermal [13, 56, 57], Ion exchanges [58–60], Microwave [15, 61, 62], Spark Plasma Sintering [63, 64], solution combustion [65] and the relatively new Pechini–type Sol-Gel [66], among others.

9.3.1 Sol-Gel Method

This method is found to be better in most cases because the mixing of the components is achieved at a molecular level and is the most successful technique to get very fine powders, low sintering temperature and Na and P

losses are minimized or completely avoided [67]. Further, it has the ability to achieve oxygen and ionic stoichiometry during the formation reaction, there is ease of synthesizing complex compositions, single phase materials, formation of higher purity products through the use of high purity reagents [68, 69], and to provide coatings over complex geometries including the insides of tubes. These advantages, however, are to be viewed in balance with the raw materials' high cost, the long processing time involved, the non-uniformity of the films, and the formation of cracks upon drying [69]. The principle of sol-gel technique consists of converting the sol, a suspension of colloidal or polymeric particles in a solvent, into a semisolid phase known as gel.

9.3.2 Hydrothermal Method

This is a low-temperature route for synthesis of ultra fine powders of NZP [25]. Hydrothermal synthesis is considered as a high-temperature technique, even though the temperatures are low compared to most traditional melt techniques. It has the advantage of rapid growth rates because of the rapid diffusion processes and it is a method of growth technique from liquid solution with lower viscosity of liquid [70]. Further advantage is that reactions do not require much time compared to conventional methods and compounds that have elements with an unusual oxidation state can be synthesized [71].

9.3.3 Ion Exchange

Solid electrolytes are ideal materials for carrying out ion exchange reactions since they have mobile ions of one type within a rigid host framework. With ion exchnage methods, new materials can be synthesized that, thermodynamically, are metastable and could not be synthesized by other means, such as direct reactions of the components [59]. Some of these new materials may have proprties or structures that are of technological importance.

9.3.4 Microwave Synthesis

A more effective method of synthesis has been proposed using microwave heating, which results in products exhibiting high phase purity, good crystallinity, and minimal loss of volatile constituents. It has been used to prepare NZP compositions [15, 61, 72], Alumina, Ziconia, ZnO, among others. It is low cost, has high heating rates, low sintering time, uniform and volumetric heating, low temperatures and improved mechanical properties, among others [73].

9.3.5 Spark Plasma Sintering

NASICON has been prepared by the Spark Plasma Sintering (SPS) method with the promise of lots of advantages. In other to activate mass transport during sintering process, the application of a current, that is electrical discharges between the particles under pressure through the sample during heating, presents a promising technique for rapid densification of ceramics at relatively low temperatures to almost the theoretical density [63]. This is the most novel and increasingly used method, which has clear advantages over the conventional sintering method that makes it possible to sinter nanomeric powders to near full desification with little grain growth [64].

9.3.6 Solid State Synthesis

Generally, inorganic solids are prepared by the reaction of a solid with another solid, a liquid or a gas usually at high temperatures. Solids do not react with each other at room temperatures; high temperatures are required to reach the suitable reaction rates. Generally, two-thirds of the melting temperature of one component is enough to activate diffusion sufficiently and to enable solid state reaction [74]. The advantages of solid state reaction are the availability of precursors and low cost for powder production on the industrial scale. The disadvantages of the solid state reaction method are that undesirable phases may be formed, the homogenous distribution of dopants is sometimes difficult to achieve, and there are limited opportunities for *in situ* monitoring of the progress of the reaction; instead, physical measurements, such as XRD, are periodically carried out. This difficulty results in mixtures of reactants and products frequently obtained. The separation of the desired product from these mixtures is generally difficult, if not impossible [74]. Further, in many compounds the reaction temperatures cannot be raised as high as necessary for reasonable reaction rates because one or more component of the reacting mixture may volatilize. Detailed description of solid state reaction theory and other methods have been discussed [74] and experimental details and results of the solid state synthesis of $NaZr_2(PO_4)_3$ have been reported [75].

9.4 NASICON Structure and Properties

The structure of NZP is such that the Na^+ is located in the interstitial sites in the framework and ionic conduction takes place when Na^+ ions move from one site to another through bottlenecks formed by oxygen ions [76]

with a strong covalent bond. The total electrical conductivity strongly depends on the density and nature of the grain boundaries. NASICON compounds exhibit a few crystalline forms depending on temperature and composition. The structural formula of NASICON can be written as $[M'_1][M''_3][A_2^{VI}][B_3^{IV}]O_{12}$, where M'_1, and M''_3 are interstitial sites occupied partially or fully by Na or other substituting ions. A and B lattice sites are primarily occupied by Zr and P or by possible substituting ions. The crystallographic structure of the parent composition $NaZr_2(PO_4)_3$ was first determined by Hangman and Kierkgaad [77] in 1967. NASICON is a solid solution derived from $NaZr_2(PO_4)_3$ by partial replacement of P by Si, with Na excess to balance the negatively charged framework [58]. The network structure of NASICON can be modified by using double phosphates and silicates to give the general formula $Na_{1+x}Zr_2P_{3-x}Si_xO_{12}$ ($0 \le x \le 3$). In the skeleton of the complex anion $(Zr_2P_{3-x}Si_xO_{12})^{(1+x)-}$, each ZrO_6 octahedron shares its six corners with tetrahedra of PO_4 or SiO_4, and each tetrahedron shares its four corners with the octahedron. Thus each O^{2-} bonds strongly to a tetrahedral and an octahedral cation. The compound has two symmetries in the range $1.8 \le x \le 2.2$, the material is monoclinic with space group *C2/c*; the rest of x yields rhombohedral unit cells of the $R\bar{3}c$ space group at room temperature, with the x = 2 having the highest conductivity [78]. At higher temperatures (~473 K), NASICON takes the rhombohedral symmetry in the entire x-range and a phase transition involving rearrangement of Na^+ ion sublattice occurs. The geometrical features of the skeleton and its interstitial space therefore satisfy the criteria for fast Na^+ ion transport. Figure 9.1 shows the structure of NASICON with the $Na1^+$ ions in the interstitial sites within the ZrO_6 octahedron and PO_4/SiO_4 tetrahedra, while Figure 9.2 is the structure of NZP, with the atomic positions of various atoms shown. The oxygen is seen bridging the P and Zr polyhedra. The counter ion $Na1^+$ is located in the specific M(1) site inside the framework.

Another way of representing the general structural formula of NZP in order to reflect the atomic sites is simply M(I), M(II), M(III) $A_{2n}(XO_4)_{3n}$, in which $[A_{2n}(XO_4)_{3n}]^{m-}$ is the rigid framework and M(I), M(II), and M(III), the three distinct empty sites in the framework. In compounds with the highest symmetry ($R\bar{3}c$), the MI site has three symmetries and coordination number is 6 and lies on the c-axis and is generally fully or partially occupied [82]. The M(II) site has two symmetries and the coordination number is 14 and it lies between the columns and is connected to the M(I) site allowing ionic conductivity.

The Na^+ cations may occupy the M(I) sites while the M(II) sites, situated outside the chains-polyhedra, remain empty [17]. Further, as the M(II) site is very big, in some cases two cations may fit into the site. The M(III) site is

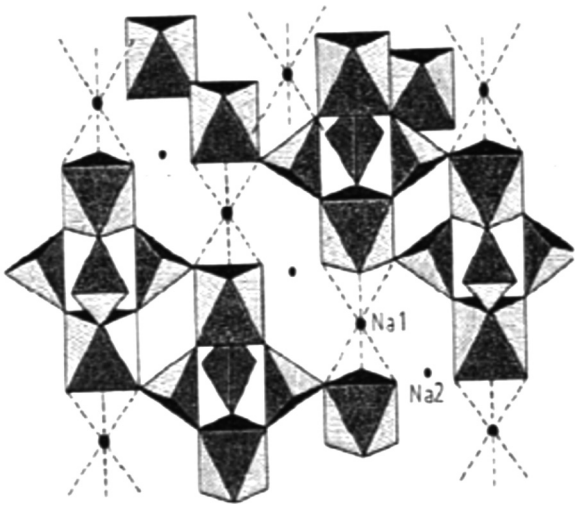

Figure 9.1 View of the rhombohedral $R\bar{3}c$ structure of NASICON showing (ZrP_3O_{12})-units parallel to c axis and Na^+ ions in Na1 positions (interstices) octahedrally coordinated by O^{2-} ions. The Na1 positions are also octahedrally coordinated by empty Na2 positions in the same basal planes as the nearest-neighbor O^{2-} ions. Reprinted from ref. [121] *Solid State Ionics*, Vol. 176, K.K. Rao, G. Rambabu, M. Raghavender, G. Prasad, G.S. Kumar, and M. Vithal, Preparation, characterization and impedance study of AgTaMP3O12 (M=Al, Ga, In, Cr,Fe and Y), pp. 2701–2710, 2005, with permission from Elsevier.

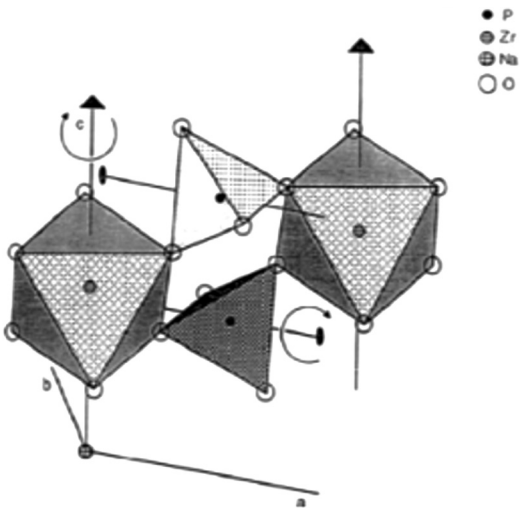

Figure 9.2 Structure of NZP showing corner shared ZrO_6 octahedra and PO_4 tetrahedra in the and the reference axes shown. Reprinted from ref. [11] R.M. Hazen, L.W. Finger, D.K. Agrawal, H.K. McKinstry and A. A. Parrotta. *Journal of Materials Research,* Vol. 2, pp. 329–337, 1987, with permission from Cambridge University Press.

a trigonal prism and has thirty-two symmetries. It can only accommodate small ions and in most cases it is empty. A and X can be substituted with many different elements, forming hundreds of different compositions [78]. For example, the M can be substituted with H^+, Li^+, Na^+, K^+, Rb^+, Cs^+, while A can be substituted with Nb^{5+}, Ta^{5+}, V^{5+}, Sb^{5+}, Ti^{4+}, Zr^{4+}, Hf^{4+}, Ge^{4+}, Sr^{4+}, and X can be substituted with A^{5+}, Si^{4+}, Ge^{4+}, S^{6+}, Mo^{6+}, Al^{3+}. Substitution of monavalent Na cation by a divalent Ca or Sr creates an ordering of cations and vacancies in the M1 sites, lowering the symmetry to $R\overline{3}$ [17]. When substitution of Na by a larger cation is made, such as by K, forming KZP, the unit cell contracts in the A lattice direction and expands in the C direction. This is also true when the Na is substituted by NH_4^+, the lattice parameter A decreases and while the C parameter increases [83]. Similarly, when the Na-O bond length increases with Ti, coupled rotations of the TiO_6 and PO_4 polyhedra lead to an expansion in the C and contraction in the A lattice directions. The different compositions give several different properties to the structure, e.g., ionic conductivity, low and negative thermal expansion, ability to immobilize radioactive nuclides, ferroelectricity, and catalytic property. The substitution of M site ions can be done at relatively low temperatures (573 K) and the framework ions A and X can be done at higher temperatures >1073 K. As the oxidation state of A and X gets higher the framework becomes stronger and the number of different substitutions to the M site increases.

Inside the framework $[A_{2n}(XO_4)_{3n}]^{m-}$, $M1^+$ counter ion fully occupy the M(I) vacancy which is located in the c-axis, between two ZrO_6. Zr^{4+} ion has radius of 0.72 Å [84]. In addition, as the $M1^+$ ion gets bigger the c-axis expands and PO_4 tetrahedra distorts. This distortion increases the O-P-O angle through c-axis and shortens the axis. In an ion exchange study [58] on $Na_{1+x}Ti_{2-x}Al_x(PO_4)_3$ (x = 0.60–0.80), where the Na was substituted by Li, two mobile ions were present in the structure and affected the lattice parameters a, c, and other physical properties like conductivity differently, depending on their position on the M sites. The Li entered the M(II) sites, which decreased the length of the lattice parameter a axis. The c axis is however more sensitive to the M(I) site composition and therefore the presence of Na in this site caused a variation of the length of the c axis upon ion exchange to be negligible. The presence of Na in the M(I) site is very important as it results in the so-called "mixed alkali effect," or "mixed cation effect," as it has been variously referred to. Since the occupancy of Na at the M(I) site is high this made the conductivity due to lithium cations highly difficult across M(I)–M(II) bottlenecks, since the Na^+ may block Li^+ diffusion along the M(I)–M(II) pathway, which may be related to the "mixed cation effect" observed mainly in glasses. A pronounced reduction in conductivity is observed in oxide glasses with two or more types of different alkali components when compared to the analogue single oxide glasses.

Lithium-conducting solid electrolytes are the most important due to the special physical properties of lithium such as its small size and low density, which leads to increased electrical conductivity on partial as well as full substitutions in the NZP system, resulting in lithium zirconium phosphate $LiZr_2(PO_4)_3$. NZP is thermally stable to 1773 K [85] whereas NASICON, depending on its composition, has melting point higher than 2073 K [86]. The substitution of Na becomes necessary since it is not a good ionic conductor for structural reasons [87]. Other compositions are obtained by replacing the Zr with Ge, Sc, In, Ti, etc., with the result that several orders of magnitude increment in conductivity at room temperature is obtained, amongst other substitutions in the P system. Some studies carried out on NZP reflect current and potential applications, such as in corrosion-resistant coating material for silicon-based ceramics and thermal barrier coatings [86]; in the development of C-C composites due to the matching of its thermal expansion properties [88] and as a nuclear waste immobilization host material [16, 89, 90]. Recently, new materials of the NZP family have been developed and structurally characterized showing high ionic conductivity and optical property, an uncharacteristic property of these compounds. Some of these include, $Na_3Al_2(PO_4)_3$ with bulk conductivity 5.0 S/m at 600 K [91], $Rb_3Yb_2(PO_4)_3$ [92], a cubic system and $Pb_{0.5}Ti_2(PO_4)_3$ [93], a hexagonal system of the $R\bar{3}c$ space group, respectively. Similarly, new NASICON-related Potassium Iron (III) Pyrophosphate has been synthesized and characterized [56], an example of which is is rhombohedral $Li_3Fe_2(PO_4)_3$, a potential electrode insertion material in lithium polymer batteries based on its good ionic conductivity and low cost [94]. The thermal expansion properties of these compounds are very important due to their relevance in the synthesis of the materials and their relationship to microstructure and density. NZP has the lowest tailorable thermal expansion coefficients and exhibit anisotropy in their thermal expansion, spurring several theoretical models to explain the thermal properties [16, 95–98] and studies on the coefficients of thermal expansion [16, 99].

Microcracking is another property that occurs in these materials due to internal stresses among grains, which results in significant lowering of strength and coefficient of thermal expansion [95]. The microcracks begin when a critical grain size of 2 μm is exceeded, which is related to the maximum thermal expansion difference between the lattice parameters [100]. In low-density ceramics, these microcracks and pores can absorb some expansion thereby causing a reduction in the thermal expansion. It has been suggested that the anisotropic thermal expansion gives rise to poor sinterability [18] and that the compositions with high degrees of thermal

anisotropy are the ones prone to microcracking upon cooling at room temperature [96], since the onset of microcracking is related to the sintering temperature and hence grain size. They suggest that microcracking may be delayed or enhanced by controlling the atmosphere in which the ceramic is heated and cooled and that thermomechanical properties in general can be improved by compositional and microstructure designs [95], all of which reflect in the way and manner the materials are synthesized. Thus the use of appropriate atmosphere is important in the characterization and performance of these materials.

9.5 Characterization Techniques

NASICON materials have been characterized by various techniques depending on the problem being investigated. Whatever the problem of investigation there are certain characterizations that are regarded as fundamental due to the information they provide about the pristine nature of the compound being investigated. The prominent ones are X-ray/neutron diffraction (XRD/ND) studies, including Rietveld analysis, which are used for phase, stoichiometry, and structural analysis. Elemental (EDX/XPS, energy dispersive spectroscopy/X-ray photoelectron spectroscopy) analysis are used for ascertaining the stoichiometry or chemical composition, including valence state in the case of XPS. Microstructure (SEM/TEM, scanning electron microscopy/transmission electron microscopy) explores the morphological features of materials, grain/grain boundaries sizes and shapes. Thermal technique such as TGA (thermogravimetric analysis) is generally used in solid state reactions to determine the sintering temperatures, i.e., decompsition temeperatures of mixtures. Typical TGA plot is shown in Figure 9.3 for $Na_{0.5}Li_{0.75}Zr_2(PO_4)_3$ between room temperature and 1273 K showing stability around 600 K. For the purposes of studies, however, techniques such as IS together with dielectric relaxation/permititvity and mobility have been used for the analysis of the electrical properties, such as ac/dc conductivity. DTA (differential thermal analysis) is used for structural /phase transformation studies in conjunction with XRD. Typical DTA plot for $Na_{0.5}Li_{0.75}Zr_2(PO_4)_3$ is shown in Figure 9.4 over a temperature range of 1273 K. No significant thermal effect is observed as earlier mentioned, except the peak around 400 K. FT-IR/Raman/NMR (Fourier Transform-Infrared/Raman spectroscopy/Nuclear Magenetic Resonance) spectroscopies are used for studies of vibrations of atoms and constituent molecules in NASICON, together with that of groups, such as phosphates or silicates, while NMR is used

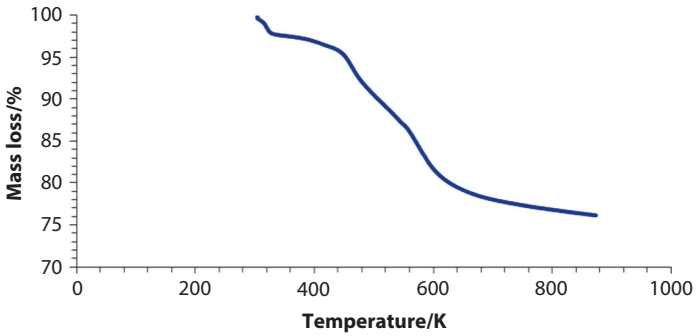

Figure 9.3 TGA plot of mass loss vs temperature (K) at different temperatures for $Na_{0.25}Li_{0.75}Zr_2(PO_4)_3$. The mass becomes stable at around 600 K [97], reproduced with kind permission from Springer Science+Business Media, *Journal of Thermal Analysis and Calorimetry*, Synthesis and thermal characterization of NZP compounds $Na_{1-x}Li_xZr_2(PO_4)_3$ (x= 0.00–0.75), Vol. 101, pp. 175–179, 2010. Ahmadu, U., A. O. Musa, S. A. Jonah and N. Rabiu, Figure 8.

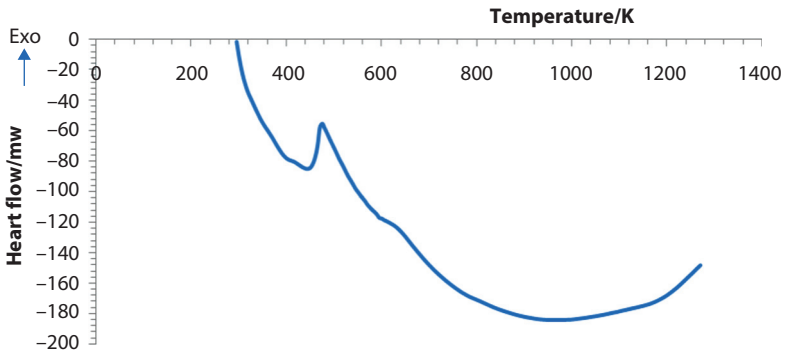

Figure 9.4 Typical DTA plot of $Na_{0.25}Li_{0.75}Zr_2(PO_4)_3$ at different temperatures with small visible peak at 201.7 K, but there is no significant thermal effect at this temperature [97], reproduced with kind permission from Springer Science+Business Media, *Journal of Thermal Analysis and Calorimetry*, Synthesis and thermal characterization of NZP compounds $Na_{1-x}Li_xZr_2(PO_4)_3$ (x= 0.00–0.75), Vol. 101, , 2010, pp. 175–179, Ahmadu, U., A.O. Musa,S. A. Jonah and N. Rabiu, Figure 4.

for transport studies: mobility and diffusion, in particular, distribution of Li ions over different sites (octahedral, tetrahedral) in the NASICON, together with activation energy and relaxation times. UV-vis spectroscopy has been used for absorption and valence state determination while Vibrating Sample Magnetometer (VSM) has been used for magnetic properties, among others.

The compound $Li_{1+x}Al_xGe_yTi_{2-x-y}(PO_4)_3$ [101] has been studied by XRD using Rietveld refinement, while $AgTaMP_3O_{12}$ (M=Al, Ga, In, Cr, Fe and Y) [79] was studied by XRD, IR and IS (impedance spectroscopy). The systems $LiTi_2(PO_4)_3$, $Li_{1.3}Al_{0.3}Ti_{1.7}(PO_4)_{2.9}(VO_4)_{0.1}$, and $A_3M_2(PO_4)_3$ (A = Li, Na and M = Cr, Fe) [65] have been investigated by XRD (Rietveld refinement), FT-IR, TEM, DSC (differential scanning calorimetry)/DTA, UV-VIS and VSM techniques. ND has been used to investigate the structural properties of $Ca_{1-x}Ba_xZr_4P_6O_{24}$ [97], including Rietveld refinement. Similarly, structural phase transformations [34] in $Li_3In_2(PO_4)_3$ by XRD, DTA, and DSC have been reported, while [102] and [103] studied $Li_{1.3}Al_{0.15}Y_{0.15}Ti_{1.7}(PO_4)_3$ and $LiM_2(PO_4)_3$, M = Ge, Ti, Sn, Zr, and Hf by NMR for Li ion mobility. Work has also been reported [87] on $Li_{1+x}Al_xTi_{2-x}(PO_4)_{2.9}(VO_4)_{0.1}$, using ^7Li, ^{27}Al and ^{31}P NMR and ^{27}Al Magic Angle Spining NMR. Ionic conductivity [104] in $Li_{1.3}Al_{0.15}Y_{0.15}Ti_{1.7}(PO_4)_3$ by XPS has been reported. Diffusion studies on single crystals of $Na_{1+x+4y}Zr_{2-y}Si_xP_{3-x}O_{12}$, $0<x< 3$, $0<y<1$ 0 found that in some of the compositions, Na interstitial sites were not involved in the diffusion [105] process but were correlated with oxygen split positions, and thus they argue that the rigid framework picture of NASICON is not tenable. Several other studies have been reported on these and other techniques. In the following sections, we discuss in detail the most used and important techniques for NASICON characterization, electrical conductivity using IS, dielectric properties and NMR, which uses mobility and relaxation.

9.5.1 Electrical Conductivity

It is important to know how much current can be passed through an electrode-electrolyte interface since some interfaces are non-polarizable or reversible while others are polarizable or non-reversible. A non-polarizable interface thus acts reversibly to the species under consideration and both ionic and electronic species may cross the interface unobstructed. Polarizable interfaces have blocking effects on the species under consideration and to a first approximation, act like a capacitor [106]. Several methods have been used to measure ionic conductivity, including far infrared and Raman spectroscopies in which the vibrations of atoms provide hop attempt frequencies. Similarly, motional narrowing of the NMR absorption lines, among others, also provides transport information. Studies on superionic conductors have been carried out at the d.c., low, microwave, and far infrared frequencies but not much is found in radio frequency (RF) range and microwave (GHz) regions. Conductivity in microwave range through theoretical studies reveal that motion of ions through the

lattice in superionic conductors is intimately linked with microwave conductivity and thus frequency range expectedly corresponds to the time scale of ionic motion. Defects or interstitial spaces provide empty sites through which ions can migrate in a hoping mechanism in which the ions move sequentially into adjacent energy-equivalent vacant sites, or by cooperative motion of the ions. Conductivity may be fully or partly ionic, in the former it may be due to the positive and negative ion species, while in the latter case it may be due to electronic contribution due to negative electrons and positive holes that may be present. Thus total ionic conductivity may not be the true bulk ionic conductivity due to factors, such as electrode–material contact resistance, which are generally of negligible fraction of total resistance in high-resistance samples, which is useful only if it is ensured that the signal makes the electrode-material system linear. There is also the problem of grain-boundary resistance whose only solution is to carry out measurements on single crystals [25]. For most superionic conductors, the art of growing single crystals is far from developed, and measurements are therefore carried out on pressed pellets. Another factor is grain boundaries, which can either increase or decrease the conductivity, depending upon whether or not the activation energy for conduction of the grain boundary is less or more than the bulk conduction. In d.c. conduction, polarization effects at the nearby electrodes are a major problem in the evaluation of ionic transport but they are useful in separating electronic components of conductivity. Simple models [107] have been presented that explains theoretically a.c. conductivity based on relaxation concepts, which illustrate some of the features of the ionic a.c. conduction in solids and helped in clarifying their origin. The models, which are applied to NASICON materials, show how long-range motion of the charges can occur in a system composed of ions that are confined by the coulomb potentials of the neighboring ions, with the condition that the position of these neighbors can also relax. At low frequencies, the long-range displacements of carriers give the frequency independent (dc) conduction σ_0. As the frequency increases, the conductivity gradually increases and over a frequency range from mHz to GHz it is well approximated by Jonscher and Almond:

$$\sigma(w) = \sigma_0 [(1 + w/w_c)^s] \tag{9.1}$$

where w_c is the frequency of the onset of ac conduction and s is a variable parameter. This equation treats the a.c. and d.c. as independent phenomena. However, both contributions should supposedly arise from the same

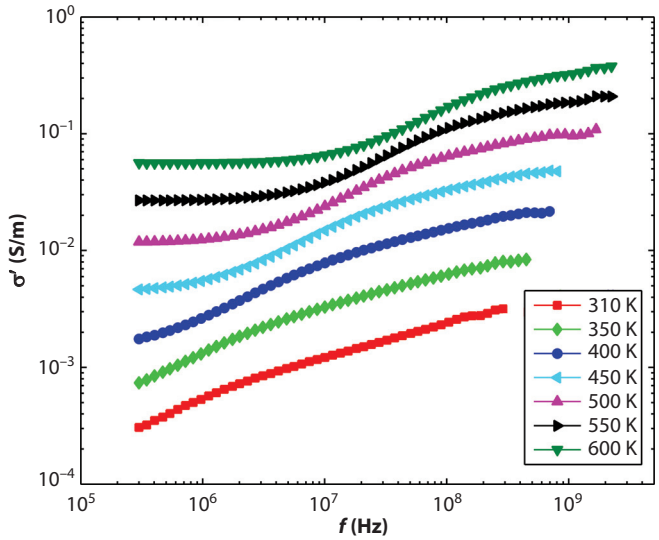

Figure 9.5 Frequency dependence of real part of complex conductivity, σ' of $Na_{0.5}Li_{0.5}Zr_2(PO_4)_3$ at different temperatures (310 to 600 K). The flat regions represent the long range d.c. conduction and the dispersive regions the the short range a.c. conduction, with frequency dependent and independent regions (d.c.). With increase in temperature the flat regions become longer which is the general behavior of ionic materials as explained by the power law of Jonscher [72].

microscopic mechanism. Another form [108] of eq. (9.1) has been provided to describe the a.c. behavior:

$$\sigma(w) = \sigma(0) + Aw^{\alpha} \tag{9.2}$$

where $\sigma(0)$ is the d.c. conductivity, A a temperature-dependent parameter and the exponent α has been found to take values between 0 and 1. This law is a universal property of the materials and is related to the dynamics of hopping conduction. Figure 9.5 shows a typical plot of a.c. conductivity at different temperatures and frequencies for $Na_{0.5}Li_{0.5}Zr_2(PO_4)3$ sytem. The flat region reperesents the long range d.c. motion, while the dispersive region is the a.c. component. Two main parameters determine conductivity: frequency and temperature. Temperature dependence is through the Arrhenius equation:

$$\sigma T = \sigma_0 \exp\left(-\frac{E_a}{k_B T}\right) \tag{9.3}$$

where σ_0 is a pre-exponential factor, σ, T, E_a and k_B are the conductivity, temperature, and Boltzmann constant, respectively. Using impedance spectroscopy the d.c. conductivity can be extrapolated based on an Argand complex plane that shows a low frequency region characterized by a straight line due to surface charge polarization and a high-frequency region due to electrical properties of the bulk. In order to determine the real part of the complex impedance (which gives the resistance and hence d.c. conductivity) the high-frequency region is approximated to a semicircle. The dc value of the resistance on the other hand corresponds to the intersection of this semi-circle and the real axis.

9.5.2 Impedance Theory and Modeling

Impedance spectroscopy (IS) is a relatively new and powerful tool for characterizing many of the electrical properties of materials and their interfaces with electronically conducting electrodes. It can be used to investigate the dynamics of bound or mobile charge in the bulk or interfacial regions of any kind of solid or liquid material: ionic, semiconducting, mixed electronic–ionic, and even insulators (dielectrics), and has been used in the study of mixed electronic ionic conductor (MIECS) coatings, bioelectrical processes, corrosion [109], and to assess the viability of the rapid chloride test for determining concrete conductivity [110]. A detailed description of the principles, theory, and experiments of IS has been presented [111]. IS measurements are carried out over a wide range of frequencies in order to identify all the time constants in the circuits, usually ten frequencies per decade are used [112] and it is a very sensitive technique since it does not provide a direct measure of physical phenomena. Other electrochemical experiments have to be carried out together with good physical knowledge of the system (microstructure), surface composition, thickness, porosity, and the presence of various layers, among others. Interpretation of impedance data requires the use of an appropriate model, a task which must be carried out very carefully. The modeling has been classified [112] as (1) physicochemical, process, or structural modeling, and (2) measurement, formal, or mathematical modeling. Process modeling links measured impedances with physicochemical parameters of the process, kinetic parameters, concentrations, diffusion coefficients, sample geometry and conditions, etc. Measurement modeling explains the experimental impedances in terms of mathematical functions in order to obtain a good fit between the calculated and experimental impedances. In the latter case, the parameters obtained do not necessarily have a clear physicochemical significance. One such modeling technique is the so-called Complex

Nonlinear Least Squares (CNLS) fitting. Experimentally obtained impedance data for a given electrode–material system may be analyzed by using an exact mathematical model based on a plausible physical theory that predicts theoretical impedance or by a relatively empirical equivalent circuit whose experimental impedance predictions are given [111]. In either the case of the relatively empirical equivalent circuit or of the exact mathematical model, the parameters can be estimated and the experimental impedance data compared to either the predicted equivalent circuit impedance or to the theoretical impedance. Analysis of experimental data that yield a full semicircular arc in the complex plane can lead to quantitative estimates of conductivity, relaxation times, and interfacial capacitance. In practice, however, experimental data are only rarely found to yield a full semicircle with its center on the real axis of the complex plane. Three common perturbations that may lead to at least part of a semicircular arc in the complex plane are: 1) the arc does not pass through the origin because there are other arcs appearing at higher frequencies; 2) the center of an experimental arc is frequently displaced below the real axis because of the presence of distributed elements in the material–electrode system. The relaxation time is then not single valued, but is distributed continuously or discretely around a mean value and the angle by which such a semicircular arc is depressed below the real axis is related to the width of the relaxation time distribution and as such is an important parameter; 3) the arcs can also be substantially distorted by other relaxations whose mean time constants are within two orders of magnitude or less of that for the arc under consideration. The experimentally obtained spectra often differ strongly from the idealized ones presented. The semi-circles may overlap and the degree of overlapping depends on the relative time constants; the closer they are, the bigger is the mixing [113]. In an ideal polycrystalline sample, the Nyquist plot (z' vs z'' exhibits an arc at high frequency, a second arc at lower frequencies, and a linear portion at the lowest frequencies, as shown in Figure 9.6.

The real and imaginary components of impedance are plotted as parametric functions of frequency; ω_0 is the relaxation frequency and $R_g(R_1)$, and C_g are the bulk resistance and capacitance, respectively while $R_{gb}(R_2)$ is the resistance of the grain boundary. The corresponding circuit model is that of two parallel RC (R_1 C_1, R_2 C_2) circuits connected in parallel together with a constant phase element Q_e (used as equivalent circuit element instead of the conventional capacitance) whose property varies from that of resistance and inductor, depending on the value of some exponents. The absence of this component has been attributed to why impedance arcs terminate at the origin [114] in some cases. Q_e represents

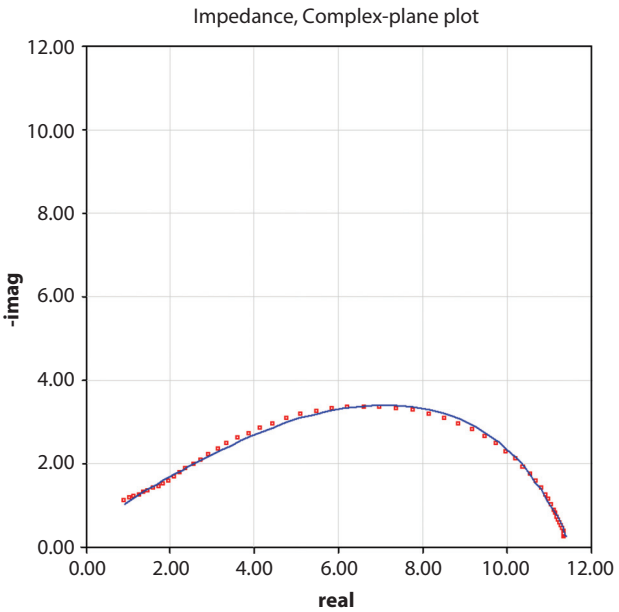

Figure 9.6 Plot of fit a nd experimental impedance data using the 'O' model equivalent circuit at 600 K based on complex non linear least squares program (CNLS).The data points are square points while the blue continuous lines are fitting results [149].

the electrode behavior, ω_0 is the relaxation frequency, the frequency at the maximum imaginary impedance. $R_g C_g$ is the time constant τ of the circuit, while the symbols represent the bulk resistance and capacitance, respectively. The measurement of the bulk conductivity is straightforward from the Nyquist plot, while the measurement of specific grain boundary conductivity requires knowledge of the grain size and grain boundary thickness. The impedance of the equivalent circuit may be approximated by:

$$Z^* = \frac{1}{\frac{1}{R_g} + i\omega C_g} + \frac{1}{\frac{1}{R_{gb}} + i\omega C_{gb}} = Z' - iZ'' \tag{9.4}$$

where

$$Z' = \frac{R_g}{1 + (\omega R_g C_g)^2} + \frac{R_{gb}}{1 + (\omega R_{gb} C_{gb})^2} \tag{9.5}$$

and

$$Z'' = R_g\left[\frac{\omega R_g C_g}{1+(\omega R_g C_g)^2}\right] + R_{gb}\left[\frac{\omega R_{gb} C_{gb}}{1+(\omega R_{gb} C_{gb})^2}\right] \tag{9.6}$$

Eq. (9.6) can be applied to the response peaks of the grain and grain boundaries which are located at $\frac{1}{2\pi R_g C_g}$ and $\frac{1}{R_{gb} C_{gb}}$, respectively. The frequency of the peaks in the z' vs z'' plots have been found based on the conditions $\omega\tau = 1$, RC = τ, and $\omega = 2\pi f$, which give $f = \frac{1}{2\pi RC}$, where ω is the angular frequency and τ is the relaxation time. The peak values are found to be proportional to the associated resistances, but in general the peak frequencies of the grain boundaries are lower than those of grains due to their large resistances and capacitances compared with those of grains. The plot of experimental impedance data on a complex plane is shown in Figure 9.7 in CNLS modeling has been used to fit the data and the grain boundary arc is seen to dominate. Figure 9.8 shows the the generic battery model fitting results for experimental data based on MEISP (Multiple Electrochemical Impedance Spectroscopy Parameterization). The results

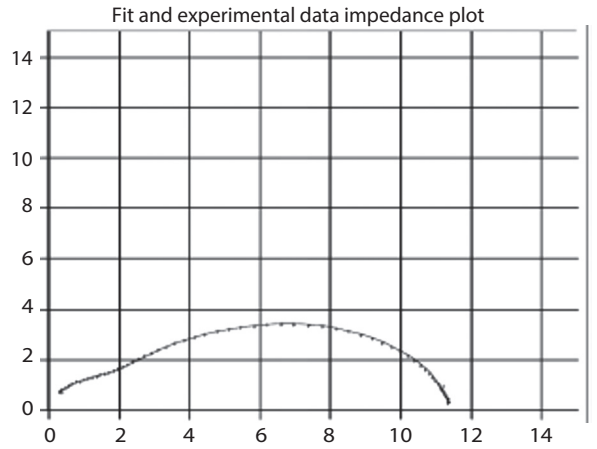

Figure 9.7 Typical fitting result of experimental data using the generic battery model of the Multiple Impedance Spectroscopy Parameterization program (MEISP) at 600 K. The fit is the continuous line while the observed data are crosses [149].

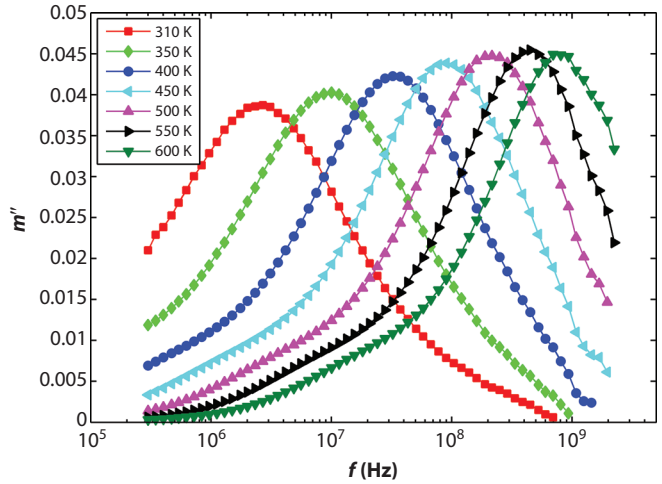

Figure 9.8 Frequency dependence of imaginary part of modulus m'' at different temperatures (310 to 600 K), showing the peaks of the relaxations shift to higher frequencies with increase of temperature [72].

show a very good fitting. Impedance data of NASICON have also been analyzed from the formalism of electric modulus, $M^* = M' + iM''$, that is,

$$M^* = M' + iM'' = i\omega C_0 Z^* \tag{9.7}$$

where, $i = \sqrt{(-1)}$, $C_0 = \varepsilon_0 \frac{s}{d}$, is the empty cell capacitance, s is the sample area and d is the thickness of the sample. Complex modulus M^* is now generally used in conjunction with the impedance and permittivity to distinguish between grain and grain boundary effects and also to understand the miscroscopic phenomena responsible for local dielectric relaxations and electrical conudctivity. Starting from eqs. (9.7) and (9.4), the corresponding equation for electric modulus representing the equivalent circuit is:

$$M' = \frac{C_0}{C_g}\left[\frac{(\omega R_g C_g)^2}{1+(\omega R_g C_g)^2}\right] + \frac{C_0}{C_{gb}}\left[\frac{(\omega R_{gb} C_{gb})^2}{1+(\omega R_{gb} C_{gb})^2}\right] \tag{9.8}$$

and

$$M'' = \frac{C_0}{C_g}\left[\frac{\omega R_g C_g}{1+(\omega R_g C_g)^2}\right] + \frac{C_0}{C_{gb}}\left[\frac{\omega R_{gb} C_{gb}}{(\omega R_{gb} C_{gb})^2}\right] \tag{9.9}$$

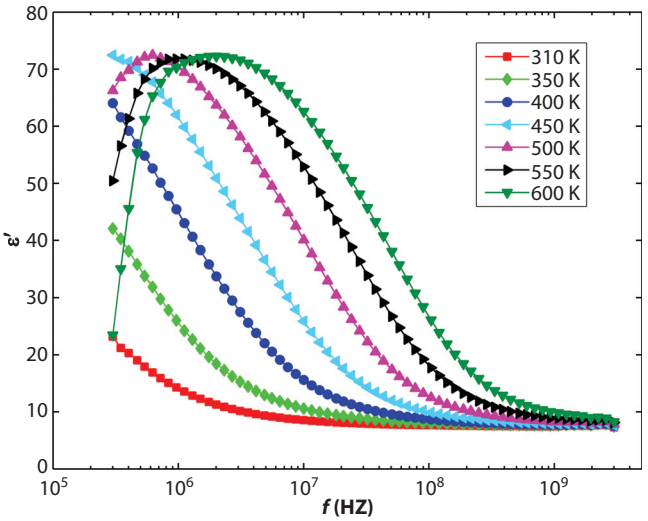

Figure 9.9 The characteristic fall in real part of dilectric permitivity ε' with increase in frequency at different temperatures (310 to 600 K) for $Na_{0.5}Li_{0.5}Zr_2(PO_4)_3$. At all temperatures, permittivity falls with frequency and peaks are observable at high temperatures [72].

Eq. (9.9) shows that there is relaxation in the M'' representation, similar to the z'' representation and the response peaks for the grains and grain boundaries also occur at frequencies $\frac{1}{2\pi R_g C_g}$ and $\frac{1}{2\pi R_{gb} C_{gb}}$, respectively. The typical plot using the modulus formalism is shown in Figure 9.9, which shows relaxations increasing to higher frequency with increase in temperature from 350 to 600 K. In order to determine the grain boundary conductivity without detailed micro-structural and electrical information, a "Brick Layer Model" (BLM) has been conventionally adopted [115]. This model is used owing to its high symmetry and the simplicity of the grain shape although its validity and limits have been highlighted [116, 117].

9.5.3 Dielectric Relaxation

For dielectric relaxation analysis, the Cole–Cole equation,

$$\varepsilon^{\star} = \varepsilon'(\omega) - i\varepsilon''(\omega) = \varepsilon_{\infty} + \frac{\varepsilon_{s-\varepsilon_{\infty}}}{1+(i\omega\tau)^{\gamma}}, \tag{9.10}$$

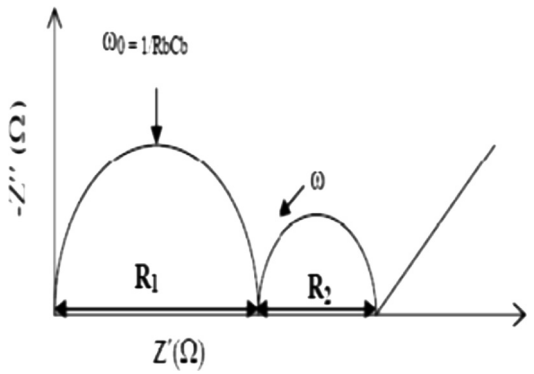

Figure 9.10 A is a typical Nyquist plot (z'' vs z') for a polycrystalline material and varies based on many parameters. The semi-circles represent the grain (R_1) and grain boundary (R_2). The inclined straight line represents electrode characteristics, Q_e, and is a constant phase element, not an ideal resistor. The frequency increases in an anti-clockwise manner. ω_0 is the relaxation frequency where R_b,C_b are the bulk resitance and capacitance, respectively.

where ε_s and ε_∞ are the static and high-frequency limits of the dielectric constant, respectively, τ is the most probable relaxation time, and γ is a constant with values between 0 and 1 are generally used for analysis. The imaginary parts of dielectric loss have been explained based on $\varepsilon'' = \dfrac{\sigma_{dc}}{\omega s_0}$, where ε_0 is vacuum dielectric constant, $\omega = 2\pi f$ is the frequency, σ_{dc} and is the dc conductivity. The dc conduction leads to further dielectric loss in addition to that due to relaxation process. The characteristic variation of dielectric permitivity ε' with frequency for $Na_{0.25}Li_{0.75}Zr_2(PO_4)_3$ is shown in figure 9.10 at diffferent temperatures.

9.5.4 Nuclear Magnetic Resonance

NMR technique has been used extensively in NASICON research for electrical and structural parameterization. The detailed theory of solid state NMR, principles, applications, and instrumentation can be found in [118] and [119]. However, here we provide a general discussion of the principles with special relation to NASICON research parameters of interest. NMR gives detailed information for selected nuclei, information about the chemical bonding, local electronic structure, orientation of a bond, measurement of distances between nuclei and the local site dynamics [119], and uses the very weak interaction between a nucleus and the rest of the universe. It has a much smaller signal-to-noise ratio compared to many spectroscopic

techniques and the weak interaction yields an extremely high resolution. Solid state NMR often employs a 200–750 MHz NMR spectrometer.

In solid state NMR nuclei, the parameters of interest are dipolar and quadrupolar coupling, chemical shift anisotrophy, Magic Angle Spining (MAS) NMR, T_1 and $T_1\rho$ relaxation, and dynamics. Chemical shift of a nucleus is due to the core and valence electrons in that nucleus and is usually described in a principal axis system in which the chemical shift tensor is diagonal and the elements contribute to the NMR spectrum via two equations [118]. In NASICON, the nuclei of interest are usually ^{23}Na (S=3/2, where S is the spin), ^{7}Li (3/2), ^{27}Al (5/2), and P (1/2). The quadrupolar interaction is described by a tensor while the electronic field gradient (EFG) is described by the size, shape, and orientation parameters. The size of the EFG tensor is given by the quadrupolar coupling constant in Hz, variously labeled C_Q or C_q, among others. The shape of the EFG tensor is given by the asymmetry parameter η. For quadrupole nucleus, the important parameters are spin and quadrupole moment, where S = 1, 3/2, 5/2, 7/2 and 9/2 are frequently encountered. The nuclear electric quadrupole moment is given by Q in units of m^2. Generally, one selects a nucleus (S,Q), then measures C_q and η as a function of structure with comparisons to calculated EFG tensors for molecular orbital calculations as C_q and η orientations, which is given by another expression for quadrupolar Hamiltonian [118].

In MAS NMR, quadrupolar and chemical shift powder patterns provide much insight into local chemical structure and dynamics. However, if the sample contains two or more nuclear sites, then the overlapping patterns can be difficult to interpret [118]. This is often resolved by MAS NMR, which consists of rapid rotation of the sample about an axis set at 54.7356° to the aplied external magetic field B_0. The MAS rotation rate is usually not fast with respect to dipolar coupling. Thus a pulse sequence, which incorporates dipolar decoupling and cross polarization is used in S = 1/2 nuclei, such as ^{31}P, to reduce the linewidth. In NMR experiments there are many relaxation paths and experiments to measure the relaxation kinetics, but the commonly used relaxations are T_1, spin-lattice relaxation, which measures the rate of energy exchange between the spin system and the vibrational and phonon modes with B_0 dependence. $T_1\rho$ is spin-lattice in the rotation frame relaxation. The most efficient spin-lattice relaxation, i.e., shortest T_1 value, occurs when the correlation time τ_{co} is approximately equal to the increase of the resonance frequency, $\tau_{co} w_o \cong 1$. When slow frequency motions are separated, i.e., moderate temperatures and high activation energies, then $T_1\rho$ at variable B_1 (where B_1 is the amplitude of the RF pulse) fields are more convinient. Other measurements have been carried out in the dynamic mode.

9.6 Experimental Results

Conductivity data for different NASICON compositions are highly variable, depending on preparation, electrode, microstructure, temperature, pressure, and mobile ion, even for the same composition. Table 9.1 is a summary of bulk electrical conductivity (σ_b, S/m), except where indicated, and activation energies E_a (eV) of some NASICON compositions at different temperatures T(K) with their references shown. The values of activation energies are the highest obtained in the various reported compositions. They are generally Li or Na ion conductors, although some higher charge ions have been found to also conduct.

In an extensive study on lithium conducting $Li_{1.3}Al_{0.3}Ti_{1.7}(PO_4)_{3-x}$(Z= V, Nb) system (LATP) [130] in which V and Nb were substituted for P, an increase in conductivity of the system was observed. Previous work shows the grain boundary component of impedance producing an arc extending to above 1 MHz down to the kHz region and literature could not provide clear information on the mechanism of conductivity enhancement, whether the grain boundary or the bulk conductivity of the system is enhanced. The nature of the electrodes was crucial in resolving the grain boundary arc in the Cole-Cole plot. They thus compared [130] graphite, silver, and gold electrodes, as well as their combinations in order to obtain well-defined impedance arcs and observed that graphite alone was too resistive, tending to dominate the impedance, whilst silver ink did not produce good adherent electrodes even though the film resistance was quite low. The best electrodes were obtained by a combination of sputtered gold layer over which silver ink was applied. Evidence of large porosity was found and showed that sintering was incomplete, hence a large grain boundary resistance was inevitable. It was demonstrated in the study of $Li_{1+x}[Al_xGe_{2-x}(PO_4)_3]$ glass-ceramics that heat treatments with shorter nucleation times leads to higher grain size and subsequently higher ionic conductivity [131]. A correlation exists between the extent of sintering and total conductivity as demonstrated in the study of two NASICON compositions [132]. Previous reports showed that the substitutions investigated led to an increment in densification, attributed to the extra intergranular low melting or glassy phases, which can act as fluxes to improve sinterability and connectivity. The use of Ar and O_2 atmospheres, however, resulted in lower conductivities. Work on Lithium-ion conducting ceramics (LATP–Lithium Aluminum Titanium Phosphate) and glasses [133] show an advantage over polymer-based systems because their conduction can be solely attributed to the lithium species. In addition, high room temperature conductivities, up to 1×10^{-1} S/m, have been reported and that the ionic conductivity can

Table 9.1 Summary of bulk electrical conductivity (σ_b **S/m)**), except where indicated, and activation energies E_a (eV) of some NASICON compositions at different temperatures T(K) with their references shown. The values of electrical conductivities are the highest obtained in the various reported compositions.

S/no.	NASICON	σ_b S/m	E_a, eV	T, K	Reference
1	$Li_{1+x}Al_xTi_{2-x}(PO_4)_3$	$1 \cdot 10^{-1}$	–	–	[140]
2	$Li_{1+x}Al_xTi_{2-x}(PO_4)_3$	$1.5 \cdot 10^{-1}$ $1.0 \cdot 10^{-2}$	–	303	[76]
3	$Li_{1+x}Al_xGe_yTi_{2-x}(PO_4)_3$, $0.2 \leq x \leq 0.8$; y = 0.8,1.0	$4 \cdot 10^{-2}$	0.37	298	[120]
4	$Li_{1+x}Ti_{2-x}Al_x(PO_4)_3$	$1.0 \cdot 10^{-1}$	–	303	[142]
5	$Li_{1.5}Ge_{1.5}Al_{0.5}(PO_4)_3$	$2.4 \cdot 10^{-2}$	–	303	[142]
6	$Li_3M_2(PO_4)_3$, M=Se, Fe, Cr	1.0	0.3–0.5	573	[54]
7	$LiTi_2(PO_4)_3$	$2.34 \cdot 10^{-4}$; $\sigma_{gb} = 7.74 \cdot 10^{-3}$	0.54 ± 0.2; 0.34 ± 0.02	298 298	[86]
8	$Li_{1.3}Ti_{1.7}Al_{0.3}(PO_4)_{2.9}(VO4)_{0.1}$	$5.32 \cdot 10^{-3}$	0.30 ± 0.01	338	[86]
9	$Li_{1.3}Al_{0.15}Y_{0.15}Ti_{1.7}(PO_4)_3$	0.42 $\sigma_{gb} = 2.5$	0.25 0.29	300 300	[122]
10	$Li_{3.2}Sc_{0.6}Z_{0.6}Ti_{1.6}(PO_4)_3$	1.2	0.33	300	[143]
11	$Na_3Zr_2Si_2PO_{12}$	$5.64 \cdot 10^{-1}$	–	1423	[98]
12	$Na_3Z_2Si_2PO_{12}$	$5.18 \cdot 10^{-1}$	–	1373	[84]
13	$Na_3Zr_{1.94}Y_{0.06}Si_2PO_{12}$	$2.1 \cdot 10^{-1}$	0.36	–	[89]
14	$Li_{1.3\ 1.7}Sc_{0.3}Ce_{1.7}(PO_4)_3$	$1.95 \cdot 10^{-3}$ $\sigma_{gb} = 1.95 \cdot 10^{-3}$	0.73 –	650 650	[144]
15	$Li_{2.25}Gac_{0.25}Ti_{1.75}(PO_4)_3$	$7.3 \cdot 10^{-2}$	0.30	303	[145]
16	$Li_{1.4}Al_{1.2}Sb_{0.8}(PO_4)_3$	$4.5 \cdot 10^{-4}$;	–	573	[134]
17	$Na_3Al_2(PO_4)_3$	5.10	–	600	[110]
18	$Li_{1.3}Al_{0.3}Ti_{1.7}(PO_4)_3$	$7.0 \cdot 10^{-2}$	–	298	[146]
19	$Li_{1.5}Al_{0.5}Hf_{1.5}(PO4)3$	$1.1 \cdot 10^{-2}$	–	–	[147]
20	$AgTaFe(PO_4)_3$	$5.11 \cdot 10^{-5}$	0.48	373	[121]
21	$Na_3Zr_{1.94}Y_{0.06}Si_2PO_{12}$	$2.15 \cdot 10^{-1}$	–	298	[89]
22	$A_3Al_2(PO_4)_3$, A=Na, Li	$7.7 \cdot 10^{-7}$;	0.72	423	[148]
23	$Na_{0.5}Li_{0.5}Zr_2(PO_4)_3$	0.25	0.36	580	[72]
24	$Na_{0.25}Li_{0.75}Zr_2(PO_4)_3$	0.3	0.36	600	[149]

be altered by controlling the channel sizes via one or more substitutions (Al, Sc, Nb, and V) since the lattice dimensions depend on the size of the structural cations. Using NMR technique, changes in ionic conductivity were observed by measuring the mobility of Lithium ions by ^{7}LiNMR. With increasing V content, the ^{7}Li static line width was found to steadily increase, indicating a decrease in lithium ion mobility [133]. The authors subsequently predicted that V substitutions in LATP will not enhance the bulk conductivity of the electrolyte.

The study of Li_xMPO_4(M = Mn, Fe, Co, Ni) [134] with NASICON structure in Ar atmosphere using 4-probe conductivity measurement showed that higher sintering temperature of the sample at 1123 K ensured higher sample density. Three of the undoped samples showed different values of conductivity and were attributed to the measurement method. The differences in the absolute values of carrier concentration were attributed to heat treatment conditions. Computed activation energies for all samples were within 0.39–0.50 eV, pointing to a common mechanism of conduction due to its narrow range. The use of blocking electrodes in d.c. measurements was found to make the conductivity predominantly electronic. IS study of NASICON in aqueous solution (0.1M NaCl for different times) using Randle's equivalent circuit for modeling and ion exchange method [135] found three semi-circles in the impedance plots: the first at high frequency (HF), which they attributed to the bulk electrical properties of the material and to inhomogeneity of the sample, since it did not show an ideal semi-circle shape but a flattened one. The second one at medium frequency (MF) was attributed to the NASICON/solution interface process, which was also not a perfect semi-circle, but became flatter when the ion exchange time increased. The third semi-circle at low frequency (LF) was assigned to slow transport processes, such as diffusion. The bulk resistance increased while the bulk capacitance decreased when ion exchange time increased and was ascribed to leaching of Na^+ ions from NASICON, which resulted in an increase in charge carrier concentration of electrolyte. The constant phase element (CPE) exponent was found to decrease and was attributed to growth of pores in the material. Contrastingly however, the interface resistance decreased while the interface capacitance increased. This was attributed to the collection of Na^+ ions at the NASICON/solution interface.

NASICON synthesized through hot-press sintering to prepare $Na_3Zr_2Si_2PO_{12}$ [76] ceramics using the sol-gel method showed that samples obtained contain mainly monoclinic NASICON, and no ZrO_2 phase was found, no matter the sintering temperature. At the sintering temperature of 1423 K, the high ionic conductivity of the sample (3.6×10^{-1} S/m) was attributed to its highest density and least grain boundary due to the

large crystal size. A variant of the sol-gel method, the so-called "drop generation" method, is said to overcome the limitations due to conventional compacting method of ceramics that leads to structural modifications as a result of variations in size, density, and non-uniformity in shape, which in turn is caused by the processing parameters [136]. A comparison of sintering techniques by solid state reaction (conventional sintering, or CS) and "Spark Plasma Sintering" (SPS) [63] has been reported in which SPS gave dense materials with high electrical conductivity at relatively low sintering temperature of 1373 K, while the highest conductivity of 1.8×10^{-1} S/m was achieved for the stoichiometric SPS composition, a value that is comparable to the best results reported in literature, 2.0×10^{-1} S/m. With increments of sintering temperature, the dc conductivity improved and reached 5.64 $x10^{-1}$ S/m at 1423 K, higher than reported results. The sintered NASICON ceramics' grain boundary impedance dominated due to its very small crystallite size, while the density of the sample sintered at 1273 K was the lowest and crystallite size the smallest, thus the ion conductivity of the sample is the lowest. A similar comparative study carried out on different zirconia precursors to evaluate their effect on electrical properties of NASICON ($Na_3Si_2Zr_2(PO_4)_3$) and NASICON-TZP ($Na_3Zr_{1.94}Y_{0.06}Si_2PO_{12}$) [67] shows that NASICON exhibits different grain sizes and the presence of a liquid phase was confirmed, which suggests high sintering temperature resulting in low temperature ion-blocking phenomenon. The NASICON-TZP has the advantage of sintering to full densification at lower temperatures. The computed conductivities and activation energies for the NASICON and NASICON-TZP are respectively, 4.10^{-2} S/m at 0.39 eV, and $2.1.10^{-1}$ S/m at 0.36 eV at room temperature. Correlation studies [40] have been carried out in which the sintering temperature, time, density, and cooling mode (air or furnace) were related to conductivity on the so-called Hong *et al*. NASICON, $Na_{1+x}Zr_2Si_xP_{3-X}O_{12}(0<x<3)$ (H-type), and Von-Alphen-type NASICON, $Na_{1+x}Zr_{2-x/3}Si_xP_{3-x}O_{12-2x/3}$, (A-type) with little ZrO_2 second phase. Most sintered NASICON contain certain amounts of ZrO_2 second phases and have a monoclinic-tetrahedral phase transition at 1373 K, below the usual sintering temperature of NASICON. The monoclinic-rhombohedral phase transition of crystalline NASICON around 473 K has been associated with a dilatometric anomaly unfavourable for applications [40]. One suggestion to overcome the problem is to effect modifications in the compositions in order to improve its microstructure and physical properties. Impedance measurements carried out at different frequencies, together with conductivity measurements, found significant changes in the activation energy for Na^+, the highest of which occurred at about 473 K, attributed to the structural change between monoclinic (*C2/c*) and

rhombohedral ($R\bar{3}c$) crystal systems, as against a second-order transition that has been suggested.

NASCON-type materials, $LiM_2(PO_4)_3$ (where M = Ge, Zr, Ti) have been studied with $Li_{1.3\,1.7}Sc_{0.3}Ce_{1.7}(PO_4)_3$ synthesized by solid state reaction [124] where the low frequency dispersion regions were attributed to blocking Pt electrodes at 650 K.The values of total (σ_t) and grain (σ_g) conductivities were found to be $\sigma_t = 8.59\times10^{-4}$ S/m and $\sigma_g = 1.95\times10^{-3}$ S/m respectively, and corresponding activation energies, E_t =1.34 eV and 0.73 eV, respectively. Conductivity studies of $LiTi_2(PO_4)_3$ ($\sigma_g \sim 10^{-4}$ S/m at room temperature) show that it could be increased by at least two orders of magnitude upon partial substitutions of Ti^{4+} by trivalent cations Al, Ga, In, Sc, Y, La, Cr, or Fe [58]; the increase is attributed to a higher charge carrier number resulting from lower porosity of the pellets. The conductivities of $Li_{1+x}Ti_{2-x}Al_x(PO_4)_3$ are as high as 10^{-1} S/m at room temperature and are due to the fact that the ionic radius of Al^{3+} is likely to lie within the tolerability limit of the NASICON framework. The maximum amount of Ti that could be replaced with Al^{3+} with the concomitant insertion of Li to balance the charges is 0.4 per formula unit. A similar study of Lithium-ion conductor $Li_{1.3}Al_{0.3}Ti_{1.7}(PO_4)_3$ showed high ionic conductivity based on novel method of preparation, even at low temperatures [137].

The compounds $LiM_2(PO_4)_3$ (M = Ge, Zr, Ti) of the NASICON-type structure have high ionic conductivity when Zr^{4+} in the $LiZr_2(PO_4)_3$ was replaced by a smaller Ti^{4+} ion [123], a phenomenon attributed to the suitability of the tunnels and size in the $LiTi_2(PO_4)_3$ for Li ion migration. Partial substitutions of Ti^{4+} by Sc^{3+} and Cr^{3+} ions in the NASICON-type structure of $LiTi_2(PO_4)_3$ is said to also cause an increase of the value of the Li ion conductivity of the substituted systems. Substitution of Zr^{4+} by Ti^{4+} and trivalent ion Sc^{3+} in the compound causes a drastic increase of σ at room temperature in comparison to the values of ionic conductivity of $Li_{1+x}Zr_{2-x}Ti_x(PO_4)_3$. The room temperature value of σ for $Li_{1+1.2}Sc_{0.6}Z_{0.6}Ti_{1.6}(PO_4)_3$ is 1.2 S/m and increases with temperature with activation energy E_g = 0.33 eV. The crystal structure of $LiZr_2(PO_4)_3$ depends on the technological condition of its preparation because the X-ray pattern of sample prepared at 1323–1373 K greatly differed from rhombohedral, and is thought to possibly correspond to a triclinic cell [123]. Similarly, $Li_{1.3\,1.7}Sc_{0.3}Ce_{1.7}(PO_4)_3$ studied by XRD, SEM, and IS [123] reported σ_t and σ_{gb} (grain boundary) conductivities at 650 K to be $8.59\cdot10^{-4}$ S/m and $1.95\cdot10^{-3}$ S/m, respectively. The space represents difficiency in the structure (non-stoichiometry). The characterization of $Li_{1+4x}Ti_{2-x}Nb_yP_{3-y}O_{12}$ (x = 0.1, 0.2, 0.3; y = 0, 0.1, 0.2, 0.3) by XPS, XRD, and IS has been reported [126] and the total conductivity of $Li_{1+x+y}Al_x(Y_y)Ti_{2-x-y}(PO_4)_3$ at 298 K was

found for the systems $Li_{1+x}Al_xTi_{2-x}(PO_4)_3$ (x = 0.3) and $Li_{1+y}Y_yTi_{2-y}(PO_4)_3$ (y = 0.4) to be $7{\cdot}10^{-2}$ S/m and $6{\cdot}10^{-2}$S/m, respectively [102].

Lithium hafnium phosphate ($LiHf_2(PO_4)_3$) (LHP) has a very high lithium ion conductivity compared to NASICON-type $LiM_2(PO_4)_3$ (M^{IV} = Ge, Sn, Ti, Zr) owing to the presence of highly mobile lithium ions [127]. The Hf^{4+} ion is more stable toward a lithium metal and reductive gases than the Ti^{4+} ion, which is an additional advantage for battery applications, though most works have been carried out on LTP ($LiTi_2(PO_4)_3$) systems due to the poor sinterability and controversial phase transitions with susbstitution in the LHP system [127]. However, it has been demonstrated that NASICON-type $Li_{1+x}[Ta_{1-x}Ge_xAl](PO_4)_3$ could be a prospective candidate for all solid state batteries since Ta and Al-oxides and phospshates are inert to chemical attack by Li metal or alloys, unlike Ti^{4+} compounds [82].

At 1423–1473 K, however, sintered $LiZr_2(PO_4)_3$ pellets belong to rhombohedral symmetry and at room temperature the value of ionic conductivity is lower than 10^{-7} S/m. Two dispersion regions, which shift toward higher frequencies with increase of temperature, were observed in all the investigated samples: a high frequency part attributed to the relaxation time in grains and a low frequency region corresponding to grain boundary processes, which are thermally activated [123]. A study of NASICON-type $Li_{1+x}Ga_xTi_{2-x}(PO_4)_3$(x = 0.1–0.9) show maximum conductivity of 7.3×10^{-2} S/m at 303 K and activation energy of 0.30 eV for $Li_{1+1.25}Ga_{0.25}Ti_{1.75}(PO_4)_3$ [125], and the addition of Li_3PO_4 or TiO_2 (rutile-type) as binder did not increase the conductivity in all the samples. This indicates the added materials have no effect on the values of the measured parameters, even though such phases may be present in the compound. Elecrical properties of new NASICON-type $Li_{3-2x}Al_{2-x}Sb_x(PO_4)_3$ (x = 0·6 to 1·4) [114] show Cole–Cole plots without any spikes on the lower frequency side, indicating negligible electrode effects. A maximum conductivity of $4{\cdot}5 \times 10^{-4}$ S/m at 573 K was obtained for x = 0·8. The presence of a single peak in the plots of both log f vs. z″ and log f vs. M″ is said to indicate bulk conductivity and absence of any grain boundary contribution to impedance. While frequency variation of conductivity, which showed two shapes at all temperatures were suggested, low frequency and low temperature conductivity, to be due to intrinsic defects and charge agglomerations present in the sample. The variation of slope with conductivity at lower frequency, on the other hand, is an indication of presence of such defects.

Lithium mobility in $LiM_2(PO_4)_3$ compounds, M = Ge, Sn was investigated by ^{7}Li NMR spectroscopy [103] in the temperature range 100–500 K. Analysis of the NMR quadrupole intensities, C_q and η parameters, spin-spin T_1 and spin-lattice T_2 relaxation rates, stuctural sites occupancy

and mobility of lithium show that below 250 K, Li ions are preferentially located at M (1) sites in rhombohedral phases but occupy intermediate M (1, 2) sites (between M (1) and M (2)) in triclinic phases. Whereas in high temperature rhombohedral phase, a superionic phase was achieved when residence times at M(1) and M(1, 2) sites become similar and correlation effects on Li motion decreases, which are due to large order-disorder transformations in rhombohedral phases or to sharp first order transitions in triclinic phases. The presence of two relaxation mechanisms in T_1 plots of rhombohedral phases were attributted to departures of conductivity from Arrhenius behavior.

The presence of only one Li site in the lattice of $Li_{1.3}Al_{0.15}Y_{0.15}Ti_{1.7}(PO_4)_3$ [102] with spin-lattice relaxation time T_1 showing only one ion motion (E_a = 0.14 eV, $\tau_0 = 6 \cdot 10^{-12}$ *s*,) has been reported. The T_1 of ^{7}Li and of ^{6}Li at room temperature were 6 ms and 2 s, respectively, which showed that the relaxation of the ^{7}Li nucleus occured through quadrupolar fluctuations while the relaxation of the ^{6}Li occured through dipolar interactions. The MAS experiments were caried out at room temperature while dynamic studies were carried out on static samples without spining. The ^{7}Li spectrum and relaxation times T_1 were measured as a function of temperature between 170 and 420 K.

Studies of ^{7}Li and ^{31}P nuclei in the temperature range 150–900 K for $Li_{1-x}La_{x/3\ \ 2x/3}Zr_2(PO_4)_3$ at x = 0.8, 0.7, 0.6, and 0.3 [138] have been investigated.The spectra recorded in the MAS mode, at room temperature, showed that Li ions occupy three chemical sites, which were sensitive to the values of x but insensitive to the coexistence of the two crystallographic varieties *c*1 or $R\overline{3}c$observed in compounds with $x \leq 0.5$. The ^{31}P MAS spectra, however, were very sensitive to lithium content but also to the variety of coexistence. T_1 measurements performed in the static mode for ^{7}Li and ^{31}P showed that the ^{7}Li spin-lattice relaxation time exhibited two branches with several minima, which indicated a complex dynamics for this ion. The observation that one of these minima appeared in the same temperature range as the minimum of the ^{31}P nuclei T_1, is said to suggest strongly a cross-relaxation process between the nuclei. $T_1\rho$ measurements on ^{7}Li (static mode) were used to probe slow motion distribution of T_1.

The positions of Na ions in two doped NASICON systems using ^{23}Na NMR showed a ^{23}Na spectra with the characteristic powder pattern of quadrupole interaction in $Na_{1-x}Zr_{2-x}Nb_xP_3O_{12}$ system [139], which is an indication that Na ions occupied Na (1) sites in the crystal structure. However, in the $Na_{1+x}Zr_{2-x}Mg_xP_3O_{12}$(x = 0.0), system, Gaussian lineshapes were observed due to the distribution of quadrupole parameters, with the occupation of both Na (1) and Na (2) sites in the system confirmed.

MAS NMR for the system $A_3Al_2(PO_4)_3$ (A = Na, Li) for ^{31}P, ^{27}Al, ^{23}Na, and ^{7}Li [128] showed that Al was the most abundant in octahedral environments, in the form of AlO_4. While the ^{31}P was ascribed to the 1Al and 2Al environments with spining satellite bands and the ^{23}Na MAS NMR spectra exhibited large assymetric bands, which indicate low mobility due to its presence in different environments. The ^{7}Li MAS NMR displayed the characteristic central position with spining satellite bands while the widths suggest low mobility for the NASICON compound.

Work has also been reported [87] on ^{27}Al, ^{31}P, and ^{7}Li NMR measurements on Li ion conductivity in $LiTi_2(PO_4)_3$ structure with Al, V, or Nb metal ions subtituted for either Ti or P. The MAS NMR showed that although Al was intended for substitution at the octahedral Ti sites, additional substitutions into tetrahedral environments (e.g., P sites) occured with increasing amount of Al susbstitution. The tetrahedral susbtitution appeared to occur more readily in the presence of V in $Li_{1+x}Al_xTi_{2-x}(PO_4)_{2.9}(VO_4)_{0.1}$.Whereas similar Nb additions to replace V appeared to stifle tetrahedral substitution. Static ^{7}Li NMR spectra showed quadrupolar stucture with $C_q \sim 42$ kHz, which was largely independent of linewidth and tended to decrease with Al substitution but increased with increasing V or Nb substitution.

Investigations of $Na_{1+x}Zr_2(PO_4)_{3-x}(SiO_4)_x$ by ^{23}Na NMR [140] showed quadrupole positions of Na (1) in $NaZr_2(PO_4)_3$ at $\nu_q = 1.2 \pm 0.1$ MHz and $\eta = 0.04 \pm 0.04$, whereas those for the Na (1) and Na (2) sites in $Na_4Zr_2(SiO_4)_3$ were at Na (1): $\nu_q = 1.03 \pm 0.01$ MHz, $\eta = 0.84 \pm 0.7$; Na (2): $\nu_q = 0.87 \pm 0.05$ MHz, $\eta = 0.53 \pm 0.4$, with an intensity ratio for the lines ~1.3, as expected. Further, the random substitution of P atoms on their lattice sites by Si atoms, for increasing x values, led to a distribution of the parameters of the quadrupole tensors, and that increasing substitution strongly affected the asymmetry of the electric field gradient.

Studies of Na positions in doped NASICON solid solution $Na_3Zr_{2-x}Y_xSi_{2-x}P_{1+x}O_{12}$ by ^{23}Na NMR [141] showed that the surroundings of the Na cations were different for different compositions and the network structures were disordered by replacement of Y^{3+} by Zr^{4+} ions in the crystal structure. But as x increased, the surroundings of the Na cations changed and the positions of the Na cations became only of one kind at x = 1.2.

NASICON-related phosphates of the type $Na_{(1+x)}Cr_xM_{(2-x)}P_3O_{12}$ (M = Ti, Hf, Zr), and $A_{(1+x)/2}Cr_xZr_{(2-x)}P_3O_{12}$ (A = Cd, Ca, Sr) [142] were studied, together with the polarizing effect of the two different metal ions A and M on the phosphorus atom and the P-O bond by both ^{31}P MAS NMR, XRD, Rietveld refinement and infrared spectroscopy. The electron density on the phosphorus, and thus the strength of the P-O bonds, were found to be affected by the interstitial (A) and structural (M) metal ions.

9.7 Problems, Applications, and Prospects

The above discussion, although basically limited by space to electrical properties, with a view to applications in solid electrolytes, did not cover many other useful potential applications and emerging trends. NASICON has generally low dielectric permitivity of ~100 and above, compared to barium titanate compositions, which are preferred. It exhibits ferroelectric phase transitions at certain temperatures and thus needs further investigations. Similarly, NASICON does not exhibit good optical properties suitable for applications, but with variations in microstructure and appropriate doping, this can be improved. However, the excellent thermodynamic and thermal properties have been relatively studied [143, 144] due to the potential application as thermal barrier coatings and heat filters. It is a very good host for immobilization of chemical wastes, apart from nuclear wastes, due its high corrosion resistance and therefore open for further investigations and improvement. The viability of using NASICON membranes as Low Activity Waste recycling has been demonstrated several times by CERAMATEC [145, 146]. In terms of its energy applications as electrodes and electrolytes, $Li_3V_2(PO_4)_3$ is a highly promising electrode material if problems like corrosion and thermal stability are worked out [147]. One significant area in which progress has been made recently is in fabrication of NASICON-based gas sensors. There is a need for chemical sensors that work in extreme conditions and which must be stable at high temperatures, all of which are easily fulfilled by NASICON with SO_x, CO_2 sensors, and polymer-NASICON composites being fabricated and demonstrated successfully [148–152].

On the theoretical front, however, progrees is also being made. The issue of alkali ion disorder in NASICON over the available sites is being debated with contradicting results, such as the case for (Na, Li) $FeTi(PO_4)_3$, $Na_2FeZr(PO_4)_3$, [153] and $A_{0.5}SbFe(PO_4)_3$ [154]. What is the solubility limit of alkali in NASICON and how far can the substitutions of various atomic radii into the host go? This is not a settled question either as it seems to depend on composition, among other factors, even though it is asserted that the largest transition metal ion soluble in NZP is dysprosium [155], but again it is arguable. Various battery model parameters (voltage, stability, and diffusion) have been optimized and compared for Li- and Na-ion systems [156]. Recently, a new modeling approach for impedance spectra analysis has been proposed, which gives more accurate results than previous ones [157, 158]. We seem to have come close to the reality of a practical, high density/capacity and cyclability lithium ion battery based

on NASICON, as has been demonstrated recently by CERAMATEC [159, 160].There is currently work being carried out on the possibility of using NASICON for bioceramics applications due to its suitable properties in bonding to tissues, according to some preliminary studies.

9.8 Conclusion

NASICON materials are the most versatile, with unique properties and diverse applications. Although various methods of synthesis and characterization have been used in order to enhance their physical and microstructural properties, more vigourous efforts are needed in the coming years to produce better results. Areas such as thin film and nanoparticle/structure synthesis have seen little progress comparatively and need further exploration in order to explore the benefits of minaturization through nanotechnology. Ferroelectric and optical properties of the materials are key areas that lacked attention and subsequently produced little positive results. The application of NASICON for large-scale energy production, cheapness, and environmental friendliness is almost at the doorstep with CERAMATEC's recent successful prototypical demonstration.

Acknowledgments

The author expresses his appreciation to Professor Masaru Aniya, Department of Physics, Kumamoto University, Japan, for providing many of his insightful publications in the field of theoretical models of superionic conductivity. Similar gestures were extended by Professor V.I. Pet'kov, Department of Chemsitry, Nizhni Novgorod State University, Russia, on his publications on NASICON, which is immensely appreciated too.

References

1. E. Kartini, T. Sakuma, A. Purwanto, T. Kamiyama and M.F. Collins, *Atom Indonesia Journal*, Vol. 31, p. 27–34, 2005.
2. D.R. Sadoway and A.M. Mayes (eds.), *MRS Bulletin*, August 2002.
3. G. Pasciak, J. Chmielowiec and P. Bujlo, *Materials Science-Poland*, Vol. 23, pp. 209–219, 2005.
4. J. Kawamura, N. Kuwata, K. Hattori, and J. Misuzaki, *Reports of the Institute of Fluid Science*, Vol.19, p.1–2, 2007.

5. N. Nunotani, M. Sawada, S. Tamura, and N. Imanaka, *Bull. Chem. Soc. Jpn.*,Vol. 83, pp. 415–418, 2010.
6. H.J. Park, Z.A. Munir and S. Kim, *Journal of the Korean Ceramic Society*,Vol. 47, p. 71, 2010.
7. S. Sumiata, E.K. Mariyanto and A. Adi, *Atom Indonesia*, Vol., 31, pp.111–125, 2005.
8. J.L. Nowinski, M. Mrocczkwoska, J.E. Garbarczyk and M. Wasiucionek, *Material Science-Poland,* Vol. 24, 2006.
9. H. Mallick and A. Sarkar, *Bull. Mater. Sci.*,Vol. 23, pp. 319–324, 2000.
10. J. Maier, *Nature Materials,* Vol. 4, pp. 805–815, 2005.
11. C. Furusawa "Fabrication and ionic conduction of ionic conducting thin films," In T. Sakuma and H. Takahashi, eds., *Physics of Solid State Ionics*. Research Signpost, Kerala, India, pp. 273–283, 2006.
12. Y. Shimizu and T. Ushijima, Sol-Gel Processing of NASICON Thin Film Using Aqueous Complex Precursor. Institute of Technology Academic Repository. http://hdl.handle.net/10228/422.kYUTU, 2013.
13. M.K. Dongare, P. Singh and P.M. Suryavanshi, *Mater. Res. Bull.*, Vol. 27, pp. 637–645, 1992.
14. J.V. Bothe and P.W. Brown. Low Temperature Formation of NZP Ceramics. http:www.netl.doe.gov/publications/processing/03/ucr-hcbu/Brown.pdf., 2013.
15. A.H. Naik, N.V. Thakkar, S.R. Darwadkhar, K.D.S. Mudher and V. Venegopal. *Journal of Thermal Analysis and Calorimetry*,Vol. 78, pp. 707–713, 2004.
16. R.M. Hazen, L.W. Finger, D.K. Agrawal, H.K. McKinstry and A.A. Parrotta, *Journal of Materials Research*, Vol. 2, pp. 329–337,1987.
17. D.A. Woodcock, P. Lightfoot and R.I. Smith, *Journal of Materials Chemistry*, Vol. 9, p. 2631, 1999.
18. P.S. Tantri, K. Greetha, A.M. Umarji and S.K. Ramasesha, *Bulletin of Materials Science*, Vol. 23, pp. 491–499,2000.
19. V.I. Pet'kov, E.A. Asabina, A.V. Markin and N.N. Smirnova, *Journal of Thermal Analysis and Calorimetry*,Vol. 91, pp. 157–8, 2008.
20. V.I. Petkov, A.I. Orlova, I.G. Trucbach, Y.A. Asabina, V.T. Demarin and V.S. Kurazhkovskaya, *Czechoslovak Journal of Physics*,Vol. 53, pp. A639–A648, 2003.
21. G. Jasinski, P. Jasinski, B. Chachulski, A. Nowakowski, *Materials Science-Poland*, Vol. 24, p. 263, 2006.
22. S. Akbar, P. Dutta and C. Lee, *International Journal of Applied Ceramic Technology,* Vol. 3, p. 306, 2006.
23. C.S. Sunandana and P.S. Kumar, *Bulletin of Materials Science*, Vol. 27, pp. 1–17, 2004.
24. P. Mass, M. Meyer, A. Bunde and W. Dieterich. *Physical Review Letters*, Vol. 7, pp. 1528–1531, 1996.
25. P.P. Kumar and S. Yashonath, *Journal of Chemical Science*, Vol. 118, pp.135–154, 2006.

26. A.J. Battacharya, T.R. Middya and S.A. Tarafdar. *Pramana Journal of Physics*, Vol. 50, pp. 1–14, 1998.
27. M. Calleja and M.T. Dove (2004). "Calculating activation energies in diffusion processes using a *monte carlo* approach in a grid environment." in M. Mubarak *et al* eds., *ICCS 2004, LNCS 309*. Springer-Verlag, Berlin, Heidelberg, Germany, pp. 483–490.
28. N.L. Allan, G.B. Barera, J.A. Purton, C.E. Smiss and M.B. Taylor. *Physical Chemistry and Chemical Physics*, Vol. 2, pp. 1094–1111, 2000.
29. C.A.J. Fisher and H. Mastubara. Oxide ion diffusion along grain boundaries in zirconia: A molecular dynamics study http://www.eng.hawaii.edu/~ssi11/SSI-11Papers/B72/B72.pdf, 2010.
30. S. Yip, *Handbook of Materials Modeling: Vol. 1, Methods and Models,* Springer, Netherlands, 2005.
31. Z. Mao, S.B. Sinnott and E.C. Dickey. *Journal of American Ceramic Society,* Vol. 85, pp. 1594–1600, 2002.
32. E. Holmström, K. Nordlund, and A. Kuronen. *Physica Scripta*, Vol. 81, pp. 1–5, 2010.
33. F. Shimojo, "Atomic dynamics in superionic conductors, *ab initio* molecular dynamics simulations." in T. Sakuma and H. Takahashi eds., *Physics of solid state ionics*, Research signpost, Keralla, India. pp. 70–86,2006.
34. Y.K. Naganovsky and S.E. Sigaryov, *Solid State Ionics*, Vol. 50, pp. 1–9, 1992.
35. A. Zurawaski, *Physics and Chemistry of Solid State*, Vol. 7, pp. 21–24, 2006.
36. S. Ramasesha, *Resonance,?* pp. 23–24, 1999.
37. M. Maliki, M. Micoulat, F. Chaimbault and Y. Vaills, *Physical Review Letters*, Vol. 96, 2006.
38. K. Singh and S. S. Bhoga, *Applied Physics A: Materials Science & Processing*, Vol. 67, pp. 475, 1998.
39. S.-J.S. Moon, T.H. Lee, S.E. Dorris and U. Balachandran, *Journal of Ceramic Processing Research*,Vol. 9, p. 377, 2008.
40. A. Tschope, "Space Charge Layers in Polycrystalline Cerium Oxide," *Material Research Society Symposium Proceedings*, Vol. 756, 2003.
41. M. Aniya, *Journal of Physics and Chemistry of Solids*, Vol. 57, pp.1811–1816,1996.
42. P. Slater, "Design of ionic and mixed cation conductors." in S. Keay-Bright ed., *Accelerated Materials Discovery for Energy Storage and Conversion Devices*. Meeting Report. St Antony's College, Oxford, UK, 2nd–4th April, REF: UKERC/MR/MP/2007/012., UKERC Meeting Place. pp. 15–16, 2007.
43. M. Aniya, *Journal of Physical Society of Japan*, Vol. 61, pp. 4474–4483,1992.
44. M. Aniya, *Solid State Ionics*, Vol. 50, pp. 125–129, 1992.
45. M. Aniya, *Journal of Physical Society of Japan*, Vol. 65, pp. 3406–3407, 1996.
46. P. Knauth, *Journal of Electroceramics,* Vol. 5, pp. 111–125, 2000.
47. A. Grey-Weal, *Faraday Discuss*, Vol. 134, pp. 297–313, 2007.
48. I. Vitioo, Ph.D Thesis. Inst. of Solid State Physics, University of Latvia, Latvia, 1999.

49. B.J. Ward, C.C. Liu, G.W. Hunter, *Journal of Materials Science*,Vol. 38, pp. 4289–4292, 2003.
50. P.A Lessing and G. Huestis. *Journal of Ceramic Processing Research*, Vol. 7, pp.1–2, 2006.
51. S.V. Kesapragada, S. Bhaduri, S. B. Bhaduri, E. G. Baburaj, P. A. Lessing, "Preparation and Characterization of Nanocrystalline Nasicon Powders and Thin Films," in: *26th Annual Conference on Composites, Advanced Ceramics, Materials, and Structures: B: Ceramic Engineering and Science Proceedings*, Vol. 23, No. 4, 2008. DOI:10.1002/9780470294758.
52. U. Ahmadu, T. Salkus, A.O. Musa and K.U. Isah, *Open Journal of Physical Chemistry*, Vol. 1, pp. 94–103, 2011.
53. E. Traversa, H. Aono, Y. Sadaoka and L. Montanaro, *Sensors and Actuators B*, Vol. 65, pp. 204–208, 2000.
54. A. Ahmad, C. Glasgow, T.A. Wheat, *Solid State Ionics*, Vol. 76, pp. 143–154, 1995.
55. M. Kotobuki, Preparation of Li-ion conductive ceramics through a sol-gel route. 2nd International Conference on Electrical, Electronics and Civil Engineering (ICEECE'2012) Singapore April 28–29, 2012.
56. G.S. Gopalakrishna, B.H. Doreswamy, M.J. Mahendra, M.A. Sridhar, J.S. Prasad and K.G. Ashamanjari, *Bulletin of Materials Science*, Vol. 28, pp. 1–7, 2005.
57. L. Sebastian and J. Gopalakrishnan, *J. Mater. Chem.*, Vol. 13, p. 433, 2003.
58. F.E. Mouahid., M. Zahir, P.M. Maldonado-Manso, S. Bruque, E.R. Losilla, M.A.G. Aranda, A. Rivera, C. Leona, J. Santamaria, *Journal of Materials Chemistry*, Vol. 11, pp. 3258–3263, 2001.
59. R.W. Anthony, *J. Mater. Chem*., Vol. 1, pp. 157–162, 1991.
60. N. Hirose and J. Kuwano, *J. Mater. Chem.*, Vol. 4, pp. 9–12, 1994.
61. A.H. Naik, S.S. Deb, A.B. Chalke, M.K. Saxena, K.L. Ramakumar, V. Venugopal and S.R. Dharwadkar, *Journal of Chemical Science*, Vol. 122, pp. 71–82, 2010.
62. Y. Fang, J. Cheng, R. Roy, D.M. Roy, D.K. Agrawal, *Journal of Materials Science*, Vol. 32, pp. 4923–4930, 1997.
63. J.S. Lee, C.M. Chang, Y.I. Lee, J.H. Lee and S.H. Hong, *Journal of American Ceramic Society*, Vol. 87, pp. 305–307, 2004.
64. T. Hungrı, J. Galy, and A. Castro, *Advanced Engineering Materials*, Vol. 11, 2009.
65. L. Vijayan and G. Govindaraj, NASICON Materials: Structure and Electrical Properties, Polycrystalline Materials—Theoretical and Practical Aspects, Prof. Zaharii Zakhariev ed., ISBN:978-953-307-934-9, InTech,: http://www.intechopen.com/books/polycrystalline-materials-theoretical-andpractical-aspects/nasicon-materials-structure-and-electrical-properties, 2012.
66. F. Ejehia, S.P.H. Marashia, D. Haghshenasa, M. Ghaanib, A. Nekahia, Proceedings of the 4th International Conference on Nanostructures (ICNS4),

12–14 March, 2012, Kish Island, I.R. Iran. Synthesis of a New NASICON Structure by Pechini-Type Sol-Gel Method.
67. R.O. Fuentes, F.M.B. Marques and J.I. Franco, *Boletin de la sociedad Espanola de Ceramica Y Vidrio*, Vol. 38, pp. 631–634, 1999.
68. T.C. Nguyen, M.Sc. thesis, Virginia Polytechnic Institute and State University, Blacksburg, Virginia, 1998.
69. U. Ahmadu, Ph.D. Dissertation, Ahmadu Bello University, Zaria, Nigeria, 2010.
70. A. Şahin, M.Sc. Thesis, İzmir Institute of Technology, Turkey, 2004.
71. A. Rabenau, *Angew. Chem*., *Int. Eng. Ed.*, Vol. 24, pp. 1026–1040, 1985.
72. D. Agrawal, J. Cheng, Y. Fang, and R. Roy, "Microwave processing of ceramics, composites and metallic materials." in D.E. Clark, D.C. Folz, C.E. Fogar and M.M. Mahmoud, eds., *Microwave Solutions for Ceramic Engineers,* The American Ceramic Society, Ohio, USA. p. 213, 2006.
73. D. Agrawal, "Microwave sintering development spur emergence of new materials and technologies," *Industrial Heating*, June Vol. 72, 2005.
74. B. Ozmen, M.Sc. Thesis, Izmir Institute of Technology, Izmir, Turkey, 2004.
75. U. Ahmadu, A.O. Musa, S.A. Jonah. and N. Rabiu, *Journal of Thermal Analysis and Calorimetry,* Vol. 101, pp. 175–179, 2010.
76. Z. Dong-mei, L. Fa, X. Zang-Long, Z. Wang-Cheng, *Transactions of Nonferrous Metal Society of China*, Vol. 17, pp. s1156–s1159, 2007.
77. E. Breval, G. Harshe and D.K. Agrawal, *Journal of Material Science Letters*, Vol. 14, pp. 728–731,1995.
78. M.N. Kutucktu, M.Sc. Thesis, Georgia Institute of Technology, Georgia, USA, 2005.
79. K.K. Rao, G. Rambabu, M. Raghavender, G. Prasad, G.S. Kumar and M. Vithal, *Solid State Ionics*, Vol. 176, pp. 2701–2710, 2005.
80. D. Gautham, Ph.D. Dissertation, Max-Planck-Institut für Metallforschung, Stuttgart, Germany, 2006.
81. T. Chen, Preparation, thermal expansion, and dielectric properties of $MTi_4P_6O_{24}$(M = Ba, Sr): http://www.etdncku.lib.ncku.edu.tw/ETD-Searchc/view-etd?URN=etd-0674103-163524, 2013.
82. C.J. Leo, G.V.S. Rao and B.V.R. Chowdari, *Journal of Materials Chemistry*, Vol. 12, pp. 1848–1853, 2002.
83. S. Kormaneni, E. Lenain, R. Roy, *Journal of Materials Science Letters*, Vol. 5, pp.1–3, 1986.
84. W. Wang and N. Zhou, Study of Mineral Fast Ion Conductors of Al-Sm-Nasicon: http://www.eng.hawaii.edu/¬ssiII/SSI-II papers/A44.pdf, 2013.
85. P. Brown, Nanostructured Ceramics and Composites, final progress report, Penn State University, 2005.
86. W.Y. Lee, K.M. Cooley, C.C. Berndt, D.L. Joslin and D.P. Stinton, *J. Am. Ceram. Soc.*, Vol. 79, p. 2759, 1996.
87. M. Forsyth, S. Wong, K.M. Nairn, A.S. Best, P.J. Newman and D.R. MacFarlane, *Solid State Ionics*, Vol. 124, pp. 213–219, 1999.

88. D. K. Agrawal, G. Harshe, E. Breval and R. Roy, *J. Mater. Res.*, Vol. 11, p. 3158, 1996.
89. S. Nakayama and K. Itoh, *J. Nucl. Sci. Tech*., Vol. 40, pp. 631–633,2003.
90. http://library.iem.ac.ru/exper/vol10–1/151–152.pdf., 2013.
91. F. Brunet, N.Bagdassarov and R. Miletich, *Solid State Ionics*, Vol. 159, pp. 35–47, 2003.
92. J.J. Carvajal, I. Pareu, R. Sale, X. Solarus, F. Dianz and M. Aguilo, *Chem. Mater*., Vol. 17, pp. 6746–6754, 2005.
93. A. El Bouari and A. El Jazouli, *Phosporus Research Bulletin*, Vol.15, p. 136, 2004.
94. A.S. Andersson, B. Kalska,P. Jonson, L. Hagstrom, P. Nardhblad, P. Tellgreen and J.O. Thomas, *J.Mater. Chem.*, Vol.10, p. 2542, 2000.
95. Z. Biao, G. Jingkum and Z. Peinan, *Science in China* (series E), pp. 337–339,1996.
96. T.B. Jackson and W.A. Porter. Environmental microcracking of [nzp] type ceramics, http://www.osti.gov./bridge/servelets/purl/102178-4Smo9M/102178.pdf., 2013.
97. S.N. Achary, O.D. Jayakumar, S.J. Patwe, A.B. Shinde, P.B.R. Krishna, S.K. Kulshreshtha and A.K. Tyagi, *PRAMANA J. Phys*., Vol. 71, pp.941–946, 2008.
98. C. Huang, D.K. Agrawal, H.A. McKinstry and S. Limaye, *J. Mater. Res.*, Vol. 9, pp. 2005–2013, 1994.
99. D.A. Woodcock, P. Lightfoot and C. Ritter, *Chem. Commun*., pp. 107–108, 1998.
100. B. Angadi, V.M. Jali, M.T. Lagare, N.S. Kini and A.M. Umarji, *Bull.Mater. Sci.*, Vol. 25, pp.191–196, 2002.
101. P. Maldonado-Manso, E.R. Losilla, M. Martínez-Lara, M.A.G. Aranda, S. Bruque, F. E. Mouahid and M. Zahir, *Chem. Mater*.,Vol. 15, pp. 1879–1885, 2003.
102. T. Salkus, E. Kazakevičius, A. Kežionis, A. Dindune, Z. Kanepe, J. Ronis, J. Emery, A. Boulant, O. Bohnke and A.F. Orliukas, *Journal of Physics: Condens Matter* Vol. 21, p. 185502, 2009.
103. K. Arbi , M.A. París , J. Sanz, *Dalton Trans.*, Vol. 40, pp. 10195–202, 2011.
104. T. Šalkus, E. Kazakevičius, A. Kežionis, V. Kazlauskienė, J. Miškinis, A. Dindune, Z. Kanepe, J. Ronis, M. Dudek, M. Bućko, J. R. Dygas, W. Bogusz, A. F. Orliukas, *Ionics*, Vol.16, pp. 631–637, 2010.
105. H. Kohler, H. Schulz, *Materials Research Bulletin*, Vol. 20, pp. 1461–1471, December 1985.
106. E.D. Tsagarakis, Ph.D Thesis, Kiel University, 2004.
107. J. Bisquert, V. Halparn and F. Hern, *J. Chem. Phys.,* Vol. 122, p. 151101, 2005.
108. M. Vijayakumar, and S. Selvasekarapandian, *Crystal Research Technolology*, Vol. 39, pp.611–616,2004.
109. W. Lai and S.M. Haile, *Journal of American Ceramic Society,* Vol. 88, p. 2979, 2005.
110. K.A. Synder, C. Ferraris, N.S. Martys and E.J. Garboczi, *Journal of Research of the National Institute of Standards and Technology*, Vol. 105, 2000.

111. J.R. Macdonald and W.B. Johnson (2005), "Fundamentals of impedance spectroscopy." in E. Barsoukov. and J.R. Macdonald, eds., *Impedance Spectroscopy Theory, Experiment, and Applications, Second Edition,* A John Wiley & Sons, Inc., Publication, Hoboken, New Jersey, USA
112. A. Lasia, "Electrochemical Impedance spectroscopy and its applications." In B.E. Conway, J.O.M. Bockris and R.E. White, eds., *Modern Aspects of Electrochemistry, no. 32*. Kluwer Academic Publishers, New York, p. 143–231, 1999.
113. D. Vladicova, *Impedance contributions online,* Vol. 1, pp. l3-1–l3-34, 2003.
114. N. Anantharamulu, G. Prasad and M. Vithal, *Bulletin of Materials Science*, Vol. 31, pp. 133–138, 2008.
115. N. Bonanos, B.C.H. Steele and E.P. Butler, "Microstructural Models for Impedance Spectra of Materials." in E. Barsoukov and J.R. Macdonald, eds., *Impedance Spectroscopy Theory, Experiment, and Applications, Second Edition*. A John Wiley & Sons, Inc., Publication, Hoboken, New Jersey, USA pp. 1–47, 2005.
116. J. Fleig and J. Maier, The influence of the microstructure on the impedance of ceramics studied by finite element calculations: http://www.fkf.mpg.de/maier/people/fleig/webjur3.pdf., 2010.
117. J. Fleig, J. Jaminik and J. Maier, On the validity and limits of the brick layer model in impedance spectroscopy: http://www.fkf.mpg.de/maier/people/fleig/rio98b.pdf., 2010.
118. G.L. Butler, "An Introduction to Solution, Solid-State, and Imaging NMR Spectroscopy," in *Handbook of Spectroscopy*, eds. G. Gauglitz and T. Vo-Dinh, WILEY-VCH Verlag GmbH & Co. KGaA, Weinheim, 2003.
119. J. Kauppinen, J. Partanen, *Fourier Transforms in Spectroscopy,* Wiley-VCH Verlag GmbH, Federal Republic of Germany, 2001.
120. X. Xu, Z. Wien, X. Wu, X. Yang and Z. Gu, *J. Am. Cer. Soc*., Vol. 90, p. 2820, 2007.
121. J. Fu, *Solid State Ionics*, Vol. 96, p.195, 1997.
122. M. Cretin and P.J. Fabry, *J. Eur. Cer. Soc*., Vol. 19, p. 2931, 1999.
123. T. Salkus, A. Dindune, Z. Kanepe, J. Ronis, A. Kazeonis and A.E. Orliukas, *Lithuanian Journal of Physics,* Vol. 46, pp. 361–366, 2006.
124. T. Salkus, A. Dindune, Z. Kanepe, J. Ronis, A. Kezionis, E. Kazakevicius, L.J. Gaukckler, U.P. Mucke and A.F. Orliukas, *Lithuanian Journal of Physics,* Vol. 46, pp. 483–488, 2006.
125. K. Oda, S. Takase and Y. Shimizu, *Material Science Forum*, Vol. 544–5, pp. 1033–1036, 2007.
126. V. Venckute, J. Banyte, V. Kazlauskiene, J. Miškinis,T. Šalkus, A. Kežionis, E. E. Kazakevičius, A. Dindune, Z. Kanepe, J. Ronis, A.F. Orliukas, *Lithuanian Journal of Physics,* Vol. 50, pp. 435–443, 2010.
127. C. Chae-Myung, H. Seong-Hyeon, P. Hyun-Min, *Solid State Ionics*, Vol. 176, pp. 2583– 2587, 2005.
128. L. Moreno-Real, P. Maldonado-Manso, L. Leon-Reina, E.R. Losilla, F.E. Mouahid, M. Zahir and J. Sanz, *J. Mater. Chem.*, Vol. 12, pp. 3681–3687, 2002.

129. U. Ahmadu, Ŝ. Tomas, S.A. Jonah, A.O. Musa, N. Rabiu, *Adv. Mat. Lett*. Vol. 4, pp. 185–195, 2013 .
130. M. Forsyth, S. Wong, K.M. Nairn, A.S. Best, P.J. Newman and D.R. MacFarlane, *Solid State Ionics*, Vol. 124, pp. 213–219, 1999.
131. A.M. Cruz and A.C.S. Rodriques, *Ceramica,* Vol. 53, pp. 180, 2007.
132. H.B. - Kang, and N.H. Cho, *J. Mater. Sci.,* Vol. 34, pp. 5005–5013, 1999.
133. M. Forsyth, S. Wong, K.M. Nairn, D.R. MacFarlene, P.J. Newman and A.S. Best, *J. Mater. Chem.*, Vol. 8, pp. 2199, 1998.
134. Y. Nian Xu, S.Y. Chung, J.T. Bloking, Y.M. Chiang and W.Y. Ching, *Electrical and Solid State Letters,*Vol. 76, pp. A131–A134, 2004.
135. N.T. Nga, and T. Son, *Communication in Physics,* Vol. 4, pp.105–110,2004.
136. J. Judes and V. Kamaraj, *Materials Science-Poland,* Vol. 27, p.407, 2009.
137. L. Zhang, P. Chen, Z. Hu, and C. Chen, *Chin. J. Chem. Phys*. Vol. 25, p. 703, 2012.
138. M. Barré, J. Emery , P. Florian, F. Le Berre , M.-P Crosnier-Lopez and J.-L. Fourquet, *Journal of Physics: Condensed Matter*, Vol. 21, pp. 175404, 2002.
139. Y. Yue, F. Deng, H. Hu, C. Ye, *Chem Phys Lett*, Vol. 235, pp. 503–507, 1995.
140. C. Jäger, S. Barth, A. Feltz, *Chemical Physics Letters*, Vol. 154, pp. 45–48,1989.
141. Y. Yong, D. Feng, H. Hong-Bing, Y. Zhao-Hui, *Acta Phys. Chim. Sin.*, Vol. 11, pp. 484–487, 1995.
142. J.B. Frank, C. Nicola and E.S. Lesley (2006), *Solid State Ionics*, Vol. 177, pp. 2889–2896, 2006.
143. R.P. Forbes, D.G. Billing, 26th European Crystallographic Meeting, ECM 26, Darmstadt, 2010, *Acta Cryst.* Vol. A66, p. s159, 2010.
144. M.V. Krishnaiah, J. Joseph, G. Seenivasan, K.V. Govindan Kutty, *Journal of Alloys and Compounds*, Vol. 351,pp. 212–216, 2003.
145. S.H. Balagopal, R.M. Flinders, S.V. Bhavaraju, D.A. Clay, K.L. Schatten, Recycling Caustic from LAW Stream using NaSICON Membrane based Electrochemical Technology— 9127WM2009 Conference, March 1–5, 2009, Phoenix, AZ, http://www.ceramatec.com/documents/Solid-State-Ionic; A.P. Poloski, G.J. Sevigny, D.E. Kurath, M.S. Fountain, L.K. Holton, Economic Feasibility of Electrochemical Caustic Recycling at the Hanford Site March 2009, Prepared for the U.S. Department of Energy under Contract DE-AC05-76RL01830, Pacific Northwest National Laboratory, Richland, Washington 99352, http://www.pnl.gov/main/publications/external/technical_reports/PNNL-18265.pdf, 2013.
146. W.R. Wilmarth, D.T. Hob's, W.A. Averill, E. Fox, R.A. Peterson, Review of Ceramatec's caustic recovery technology, July 20.Washington savannah river company, savannah river site, Aiken, SC 29808. Prepared for the U.S. Department of Energy Under Contract Number DE-AC09-96SR18500, 2007.
147. Q. Chao-Qun, W. Ying-Jin, J. Tao, *Journal of Inorganic Materials*, Vol. 27, pp. 561–56, 2012.
148. R. Akila, K.T. Jacob, *Journal of Applied Electrochemistry*, Vol. 18, pp. 245–251, 1988.

149. S. Yao and J. R. Stetter, Solid Electrolyte Sensors for Emissions, Monitoring, http://www.electrochem.org/dl/ma/201/pdfs/1573.pdf, 2013.
150. G.W. Hunter, J.C. Xu, C.C. Liu, J.W. Hammond, B. Ward, D. Lukco, P. Lampard, M. Artale, and D. Miniaturized Amperometric Solid Electrolyte Carbon Dioxide Sensors http://ntrs.nasa.gov/archive/nasa/casi.ntrs.nasa.gov/20090014003_2009013126.pdf, 2013.
151. K.M. Nairn A.S. Best, P.J. Newman, D.R. MacFarlane and M. Forsyth, Ceramic-Polymer Interface in Composite Electrolytes of Lithium Aluminium Titanium Phosphate and Polyetherurethane Polymer Electrolyte. www4.eng.hawaii.edu/~ssi11/SSI-11Papers/C58.pdf, 2013.
152. S. Baliteaua, A-L. Sauvetb, C. Lopeza and P. Fabry, Characterization of a NASICON based potentiometric CO2 sensor, http://web1.see.asso.fr/electroceramics/html/cdrom/pdf/Papers/D08-02-Ora.pdf, 2013.
153. M. Sommariva, M. Catti, and A. Comotti, 22nd European Crystallographic Meeting, ECM22, Budapest, *Acta Cryst.*, Vol. A60, p. s258, 2004.
154. B. Haggouch, A. Aatiq, Structure and spectroscopic study of Nasicon phosphates series, First Euro-Mediterranean Conference on Materials and Renewable Energies (EMCMRE-1), 21–25 November, 2011.
155. G. Hitz, K.T. Lee and E.D. Wachsman, Synthesis and characterization of $Na_{3+x}M_xZr_{2-x}Si_2P_3O_{12}$ for solid state Na-ion battery applications, Abstract #1863, Honolulu PRiME 2012, The Electrochemical Society, http://ma.ecsdl.org/content/MA2012-02/15/1863.full.pdf, 2013.
156. S. Ping Ong, V.L. Chevrier, G. Hautier, A. Jain, C. Moore, S. Kim, X. Ma and G. Ceder, Energy & Environmental Science, DOI: 10.1039/c1ee01782a,Voltage, stability and diffusion barrier differences between sodium-ion and lithium-ion intercalation materials.
157. J. Ross Macdonald, *J. Phys.: Condens. Matter*., Vol. 24, p. 17504, 2012.
158. W. Bogusz, F. Krok, W. Piszczatowski, *Solid State Ionics,* Vol. 119, pp. 165–171, 1999.
159. Ceramatic sodium battery technology, http://swenergyforum.com/pdfs/Grover%20Coors%20-%20330pm%20breakout.pdf, 2013.
160. J. Salton, New solar battery technology offers household power at 2.5c per kWh, September 2, 2009, http://www.gizmag.com/solar-battery-cheap-power/12676/, 2013.